International Journal of Digital Earth

ISSN: (Print) (Online) Journal homepage: https://www.tandfonline.com/loi/tjde20

FORSAT: a 3D forest monitoring system for cover mapping and volumetric 3D change detection

Efstratios Stylianidis , Devrim Akca , Daniela Poli , Martin Hofer , Armin Gruen , Victor Sanchez Martin , Konstantinos Smagas , Andreas Walli , Orhan Altan , Elisa Jimeno & Alejandro Garcia

To cite this article: Efstratios Stylianidis , Devrim Akca , Daniela Poli , Martin Hofer , Armin Gruen , Victor Sanchez Martin , Konstantinos Smagas , Andreas Walli , Orhan Altan , Elisa Jimeno & Alejandro Garcia (2020) FORSAT: a 3D forest monitoring system for cover mapping and volumetric 3D change detection, International Journal of Digital Earth, 13:8, 854-885, DOI: 10.1080/17538947.2019.1585975

To link to this article: https://doi.org/10.1080/17538947.2019.1585975

Published online: 01 Mar 2019.

INTERNATIONAL JOURNAL OF DIGITAL EARTH
2020, VOL. 13, NO. 8, 854–885
https://doi.org/10.1080/17538947.2019.1585975

FORSAT: a 3D forest monitoring system for cover mapping and volumetric 3D change detection*

Efstratios Stylianidis [a], Devrim Akca [b], Daniela Poli[c], Martin Hofer[d], Armin Gruen[e], Victor Sanchez Martin[f], Konstantinos Smagas[g], Andreas Walli[d], Orhan Altan[h], Elisa Jimeno[f] and Alejandro Garcia[f]

[a]School of Spatial Planning and Development, Aristotle University of Thessaloniki, Thessaloniki, Greece; [b]Department of Civil Engineering, Isik University, Sile, Istanbul, Turkey; [c]4DiXplorer AG, Zurich, Switzerland; [d]GeoVille Information Systems GmbH, Innsbruck, Austria; [e]Chair of Information Architecture, ETH Zurich, Switzerland; [f]Ingeniería Y Soluciones Informáticas S.L., Sevilla, Spain; [g]GeoImaging Ltd, Nicosia, Cyprus; [h]Ekinoks Surveying Software Engineering Ltd, Istanbul, Turkey

ABSTRACT

A 3D forest monitoring system, called FORSAT (a **sat**ellite very high resolution image processing platform for **for**est assessment), was developed for the extraction of 3D geometric forest information from very high resolution (VHR) satellite imagery and the automatic 3D change detection. FORSAT is composed of two complementary tasks: (1) the geometric and radiometric processing of satellite optical imagery and digital surface model (DSM) reconstruction by using a precise and robust image matching approach specially designed for VHR satellite imagery, (2) 3D surface comparison for change detection. It allows the users to import DSMs, align them using an advanced 3D surface matching approach and calculate the 3D differences and volume changes (together with precision values) between epochs. FORSAT is a single source and flexible forest information solution, allowing expert and non-expert remote sensing users to monitor forests in three and four (time) dimensions. The geometric resolution and thematic content of VHR optical imagery are sufficient for many forest information needs such as deforestation, clear-cut and fire severity mapping. The capacity and benefits of FORSAT, as a forest information system contributing to the sustainable forest management, have been tested and validated in case studies located in Austria, Switzerland and Spain.

ARTICLE HISTORY
Received 27 April 2018
Accepted 19 February 2019

KEYWORDS
Deforestation; 3D; VHR satellite imagery; orientation; image matching; DSM generation; co-registration; volumetric change detection; volume precision

1. Introduction

Different technological solutions are available for multi-scale and multi-temporal acquisitions of forest data. The choice of the data collection method is the result of a balance between economy and technology. Reference literature shows that terrestrial laser scanning (TLS) is used for rapid and detailed measurement of individual tree stems (Kelbe et al. 2017; Liu et al. 2017), in spite of the fact that in such cases the canopy surface cannot be modelled comprehensively.

Advancements in unmanned aerial systems (UASs) open new possibilities in forest mapping, on the other hand, both the spatial and temporal resolutions of UAS imagery better suit local-scale investigations (Lisein et al. 2013; Jensen and Mathews 2016) with area size at hectare level. Airborne

CONTACT Devrim Akca akca@isikun.edu.tr Department of Civil Engineering, Isik University, 34980 Sile, Istanbul, Turkey
*(Extended version of a paper which was presented at the XXIII-rd ISPRS Congress, held in Prague, Czech Republic from 12-th to 19-th July 2016)

LiDAR is widely used for the reconstruction of canopy height models (CHMs) and individual tree crowns (Wang et al. 2016; Wu et al. 2016; Xiao et al. 2016) for larger areas. The performance of image-based 3D tree modelling was compared to data derived from airborne LiDAR and it was found that when the shape of canopy is required the image-based methods may deliver the better results (Waser et al. 2007; Baltsavias et al. 2008; Waser et al. 2008a). While the image matcher generates an envelope of the canopy the Laser will penetrate the tree and produces reflections from stem and branches, thus leading to a mismodelled canopy surface. The flying altitude, scanning angle, spatial resolution, system and platform type are the main factors affecting the final data quality (Keränen, Maltamo, and Packalen 2016). LiDAR data post-processing is in many cases complex, for instance, for the presence of spikes in surface models (Khosravipour, Skidmore, and Isenburg 2016; Vauhkonen et al. 2016). Separation of true measurements from solar noise is a crucial point in the processing of high altitude single photon LiDAR systems (Wastlund et al. 2018). Ground penetration property of the signal, topological errors, operational and logistical restrictions, and especially the costs are critical points, too. On the operational aspect, data management has become a bottleneck in large scale laser scanning operations (Vo, Laefer, and Bertolotto 2016).

Moving to satellite platforms, TanDEM-X elevation models are used to generate CHMs of wider areas. Anyway, X-band interferometers require external terrain data, which leads to additional costs and efforts (Schlund et al. 2016). The X-band radar has a certain penetration depth (Persson and Fransson 2016), which may cause local underestimation of the canopy surface. Finally, time series of ESA Sentinel-2 and Landsat imagery are used to monitor global forest cover and change (Feng et al. 2016; Hermosilla et al. 2016), but not at the fine detail level.

Forest monitoring and information gathering are traditionally done through expensive and time consuming field studies in combination with terrestrial and aerial surveys with optical and LiDAR sensors. This is followed by digital data analysis in image processing suites and geographic information systems (GIS) to derive basic parameters such as area coverage, species, height, volume, health, damage, change, deforestation, etc. Subsequently, the map and statistical data are used for management decisions, implementations of regulations or simply for industry operations. The range of requirements, given by forest industries and management authorities of the forest sector, calls for more direct remote sensing capacities and technologies, that can offer a high level of reliable information in a reasonable time, at fine resolution and reduced costs. Focusing on regional and national scales of application, the very high resolution (VHR) stereoscopic acquisitions from satellite platforms offer less expensive, faster and more agile remote sensing capacities than the terrestrial and aerial ones, thereby providing a complementary, single source for orthoimages and ground elevation information. In addition, satellite systems offer other advantages to aerial acquisitions, such as no overflight permissions needed, a much greater ground coverage capacity, the availability of more spectral bands and frequent repetition on a certain area of interest.

As the infrastructure investments (i.e. satellite and ground segments) have been made, the investments in the development of exploitation technologies (i.e. algorithms and processing chains), which can put the new earth observation capacities to work, are following behind. Progress is predominantly technology driven (Gruen 2008). Here, we have identified a research opportunity for the forestry sector, and executed a project to develop a new methodology and associated algorithms and software specifically designed for forest monitoring and management tasks. The project is entitled 'a **sat**ellite VHR image processing platform for **for**est assessment', namely FORSAT, which is a research and development project co-funded by Eurostars through the national funding authorities and the European Commission. Eurostars is a joint programme between EUREKA and the European Commission to support international innovative projects led by research and development – performing small – and medium-sized enterprises. The aim of the FORSAT project is to raise the current technological level of aerial photogrammetry and LiDAR to a satellite-based monitoring capacity for forest cover mapping applications. More specifically, it intends to transfer the existing precise processing capabilities of airborne techniques to VHR optical, stereographic satellite data, thereby providing a single-source geometric forest information solution.

Forest mapping and modelling is performed with remote sensing data and techniques at several levels of detail, such as TLS (Hosoi, Nakai, and Omasa 2009; Zheng and Moskal 2012), UAS (Dash et al. 2017; Sankey et al. 2017), UAS photogrammetry (Fankhauser, Strigul, and Gatziolis 2018), aerial photogrammetry (Baltsavias et al. 2008; Waser et al. 2008b), satellite SAR (Baron and Erasmi 2017; Martone et al. 2018), multispectral (Castillo et al. 2017; Chen et al. 2017), and VHR optical imagery (Meddens et al. 2018; Wagner et al. 2018), and satellite InSAR (Sadeghi et al. 2018). The VHR optical imagery is the viable option among them due to its balance between the coverage and resolution, cost and availability. The photogrammetric image matching methods have proved their capabilities against to LiDAR counterparts as shown in several airborne (Waser et al. 2007; Baltsavias et al. 2008; Waser et al. 2008a; Kukkonen, Maltamo, and Packalen 2017; Jayathunga, Owari, and Tsuyuki 2018; Navarro et al. 2018; White et al. 2018) and spaceborne comparison studies (Zhang and Gruen 2006; Gong and Fritsch 2018; Pearse et al. 2018). In FORSAT, input pipeline of the VHR optical imagery is combined with an advanced image matching method. The image matcher has the advantages of geometrically constrained multi-image matching, combination of area-based and feature-based matching, coarse-to-fine hierarchical matching and dense image matching.

Forest change is inevitable. Forest height changes (Stepper, Straub, and Pretzsch 2015; Tian et al. 2017) and area changes (Desclée, Bogaert, and Defourny 2006; Charru et al. 2017; Senf et al. 2017; Zhu 2017; Reiche et al. 2018) are well studied. In contrast, 3D changes are less studied (Tran, Ressl, and Pfeifer 2018). Volume computation is performed for timber and biomass estimation (Rahlf et al. 2014; Magnussen, Nord-Larsen, and Riis-Nielsen 2018; Puliti et al. 2018), but not for change analysis (Qin, Tian, and Reinartz 2016). In FORSAT, a fully 3D surface matching method is used to detect forest changes in terms of deforestation and regeneration. The surface matcher can compute the changes in height (1D), area (2D) and volume (3D) units. Furthermore, a theoretical precision estimation is derived and associated to each volume value.

The scientific merit of the proposed system is to have tailored the state-of-the-art 3D surface modelling workflow to the forest domain and to 3D change analysis. Indeed one tool combines advanced image and surface matching algorithms and allows experts and non-experts users to model the forest surfaces with detail, align at sub-pixel accuracy more models of the same areas and conduct accurate volumetric analysis. The FORSAT methodology, described in the next section, enables high resolution (HR) thematic mapping of forest areas along with the use of 3D canopy model, thereby allowing the derivation of forest volumes. Based on new image acquisitions as well as on historical data, the system allows automatic change detection of forest/non-forest areas along with change modelling in forest volumes. The FORSAT functionalities, accuracies, capacities and applicability to specified forest segments were tested by executing three application case studies located in Austria, Switzerland and Spain. The results achieved in the test cases are reported in the third section. Advantages and disadvantages of the proposed method are discussed in the fourth section, followed by final conclusions.

2. Technical approach

The workflow of FORSAT is graphically represented in Figure 1. The overall architecture comprises four modules: pre-processing, geo-referencing, digital surface model (DSM) generation and 3D comparison. Each module is running independently but is also tightly coupled in an object-oriented software framework.

The same workflow could be seen as a combination of two complementary tasks. The first task is the geometric and radiometric processing of satellite imagery and 2D/3D information extraction, whose steps are radiometric pre-processing, image and ground point measurement, improvement of geometric sensor orientation, quasi-epipolar image generation for stereo measurements, image matching for DSM extraction, orthorectification and orthoimage generation, and 3D point measurements in single images using monoplotting, in stereo images as well as in image triplets (Gruen, Poli, and Zhang 2004; Poli 2005; Zhang 2005; Zhang and Gruen 2006). The tool supports most of the

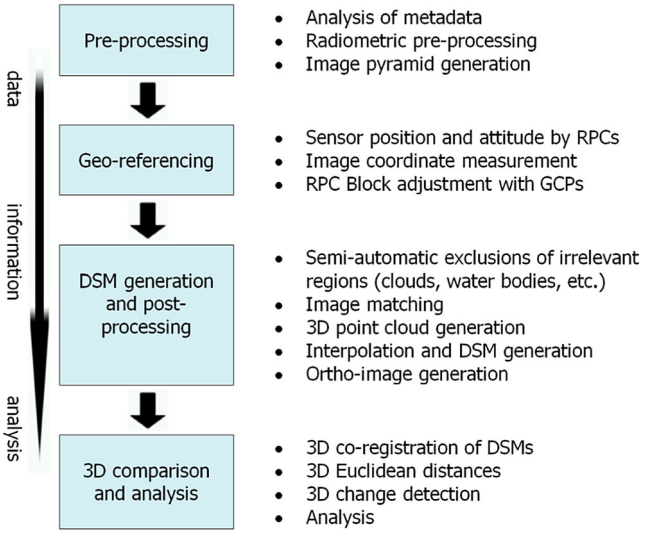

Figure 1. Main components of the FORSAT processing chain.

VHR optical imagery commonly used for civil applications, active and non-active (e.g. for historical analysis) such as IKONOS, OrbView-3, SPOT-5 HRS, SPOT-5 HRG, QuickBird, GeoEye-1/2, WorldView-1/2/3, Pléiades 1A/1B, SPOT 6/7, and sensors of similar type to be expected in the future.

The second task is committed to 3D surface co-registration, comparison and change detection. It allows the users to read DSMs and digital terrain models (DTMs), co-register them using an advanced 3D surface matching technique (Akca 2007) and calculate the 3D differences, in the form of volume changes (in m^3 units).

The origins of the orientation, image matching, and surface matching and comparison algorithms date back to the academic works performed at the group of Photogrammetry and Remote Sensing at ETH Zurich (Poli 2005; Zhang 2005; Akca 2007). Later on, these algorithms were commercialised as SAT-PP (SATellite image Precision Processing) and LS3D (Least Squares 3D surface matching) software packages by 4DiXplorer AG (www.4dixplorer.com), an ETH spin-off company located in Zurich. FORSAT is an integration, adaptation and improvement of these software packages specifically for the forestry applications.

The Ames stereo pipeline (Broxton and Edwards 2008; Moratto et al. 2010; Fassett 2016), MicMac (Pierrot-Deseilligny and Paparoditis 2006; Rupnik, Daakir, and Pierrot-Deseilligny 2017; Rupnik, Pierrot-Deseilligny, and Delorme 2018), GRAPHOS (Gonzalez-Aguilera et al. 2018) and COLMAP (Schönberger et al. 2016; Schönberger and Frahm 2016) are the general-purpose image matching software which are available in open source. SURE (Rothermel et al. 2012) and RSP (Qin 2016) are the academic examples. Correlator3D (SimActive), Pix4Dmapper (Pix4D), PhotoScan (Agisoft) and ContextCapture (Acute3D) are the commercial examples for image matching. More alternatives in orientation (Remondino et al. 2012), image matching (Gruen 2012; Remondino et al. 2014), surface matching (Akca 2010; Shean et al. 2016) and visualisation (Manferdini and Remondino 2010) do exist.

There is not a single reason which makes FORSAT more suitable over the alternatives. Rather, it has a collection of algorithmic capabilities which altogether constitute an advanced solution for deforestation analysis tasks. See the details in the fourth section.

The upcoming sub-sections explain the basic components of FORSAT system, i.e. metadata analysis, pre-processing, image pyramid generation, geo-referencing, DSM generation, co-

registration, comparison and change analysis, and precision estimation. More information can be found in Poli (2005), Zhang (2005) and Akca (2007).

2.1. Metadata analysis

The VHR satellite images include metadata information provided by the vendors in non-standard formats. Before processing the images, preliminary operations on the metadata are performed in order to prepare the input data. These pre-processing operations include both the analysis of the optical sensor (i.e. internal calibration) and image acquisition characteristics (i.e. incidence angles, sun illumination, etc.) for a better understanding of the image content, and the extraction of the required information for the radiometric improvement (Poli 2007). For the above-mentioned sensors, the metadata reading operation was successfully performed, and a strategy for the extension to other metadata formats was planned.

2.2. Image radiometric pre-processing

The performance of the image matching and feature extraction procedures depends on the quality and quantity of radiometric information being included in imagery. Compared to the traditional scanned 8-bit/pixel images, digital imagery from linear array sensors has better radiometric performance e.g. higher dynamic range and better signal-to-noise ratio. Most of the linear array sensors have the ability to provide high quality digital images. However, some radiometric problems still have to be considered: poor image contrast, image blur problems, image noise, and radiometric problems caused by the variations in the sensor view angle, the sun angle, shadowing, and the seasonal and the atmospheric conditions. These problems are usually beyond the control of the users, but their effects can be reduced by applying appropriate pre-processing methods (Zhang 2005).

Gamma correction, contrast enhancement, histogram equalisation are trivial applications and can be found in many standard image processing software. The pre-processing radiometric approach in FORSAT uses the Wallis filter (Wallis 1976), which forces the mean and standard deviation of an image to given target values. Wallis filter is successful in noise reduction meanwhile sharpening the edges and preserving small details (Baltsavias, Pateraki, and Zhang 2001; Pateraki and Baltsavias 2002; Pateraki 2005).

2.3. Image pyramids

An image pyramid is a multi-resolution representation of the original image. It is used in many of the modern matching algorithms to speed-up the image matching computation while at the same time keeping the finest spatial resolution for the final DSM output. With a coarse-to-fine hierarchical strategy based on image pyramid representation, the matches obtained at a coarse resolution are used to guide and limit the search space for the matching of finer-resolution features. In this strategy, the usual way is to start matching at a low resolution pyramid level, where the influence of image noise is reduced and coarse approximate values are sufficient to stay within the pull-in range of the matching procedure. In addition, in the low resolution images, the regions of interest for correspondence analysis in levels of higher resolution can be found at low cost because irrelevant details are no longer disturbing there. The computations are usually performed successively on each level of the hierarchy using the results of the higher level as approximate information (Ackermann and Hahn 1991; Zhang and Gruen 2006).

In FORSAT, the image pyramids are generated after the radiometric pre-processing step, starting from the original resolution images level 0, until level 3. Each pyramid level is generated by multiplying a 7×7 pixel kernel and reduces the resolution by factor 3 (Figure 2). This generating kernel size is selected due to a better approximation of the ideal Gaussian kernel (Zhang 2005). There are totally four levels, including base level 0.

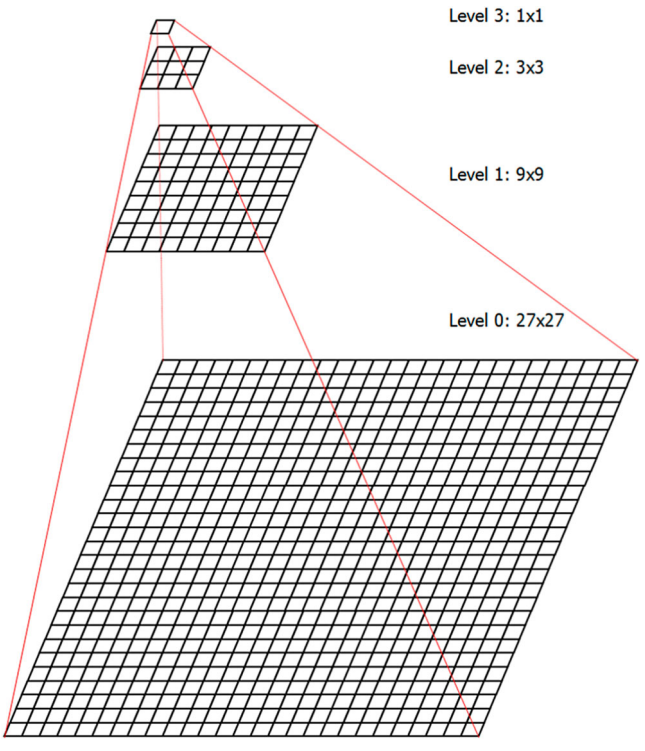

Figure 2. Four image pyramid levels in FORSAT. The level size is defined according to $3^{3-n} \times 3^{3-n}$ formula where n stands for the level number.

2.4. Image geo-referencing

The rational function model (RFM), which is a well-known non-rigorous (generalised) orientation method based on the rational polynomial functions (Kratky 1989; Toutin 2004; Kim and Dowman 2006; Poli and Toutin 2012), is used in FORSAT for geo-referencing. An RFM is the ratio of two polynomials derived from the rigorous sensor model and the corresponding terrain information, which does not explicitly reveal the sensor model parameters. The rational polynomials coefficients (RPCs), available as metadata information, are computed by image vendors by a least squares adjustment with the use of the rigorous sensor model and virtual control points (Dial and Grodecki 2002; Tao and Hu 2001).

In FORSAT, the geo-positioning accuracy of the RFM can be improved with the use of few ground control points (GCPs) (Fraser, Baltsavias, and Gruen 2002; Grodecki and Dial 2003; Zhang and Gruen 2006). This is achieved through a kind of RPC block adjustment that can accommodate stereo and triplet satellite images. It refines the orientation information if the quality of the RPCs is not given at a sufficient level. The distribution and positional accuracy of the GCPs play an essential role here. The required number of GCPs depends on the size and topography of the project area. Although just one GCP is theoretically enough for a constant correction, we recommend to use at least three points. However, it is always a good idea to use a few more for the sake of reliability and for independent quality check, of course, if accessible.

2.5. DSM generation

The automated DSM generation is performed using a modified version of the multiple primitives multi-image matching (MPIM) method (Zhang and Gruen 2004; Zhang 2005; Zhang and Gruen 2006).

It matches a dense pattern of features with an appropriate matching strategy, making use of all available and explicit knowledge, concerning sensor model, network structure, image content and geometrical constraints such as the epipolar geometry constraint (Zhang 2005; Zhang et al. 2006; Baltsavias et al. 2007).

The matching approach combines the area-based and the feature-based matching methods that are run in parallel through all the image pyramid levels in the MPIM module.

As mentioned above, a coarse-to-fine hierarchical matching strategy is followed. Starting from the low-density features on the lowest resolution level of image pyramid, the matching procedure progressively approaches the original resolution images. The triangulated irregular network (TIN) is reconstructed from the matched features on each level of the pyramid using the Delaunay triangulation method (Tarvydas 1983; Tsai 1993), which in turn is used in the subsequent pyramid level for the approximations and adaptively computation of the matching parameters. Finally, least squares matching methods are used to achieve more precise matches and to identify false matches (Figure 3; Zhang 2005).

Since the matching procedures are based on the concept of multi-image matching (two-fold and three-fold images like Pléiades triplets) guided from the object space, any number of images could be potentially processed simultaneously for DSM generation.

2.6. 3D Co-registration, comparison and change analysis

The co-registration of digital elevation models (DEMs) is crucially needed wherever spatially related datasets can be described as digital surfaces and have to be compared to each other.

There have been some studies on the co-registration of DEMs for control information and for change detection tasks. This work is known as DEM matching (Ebner and Strunz 1988;

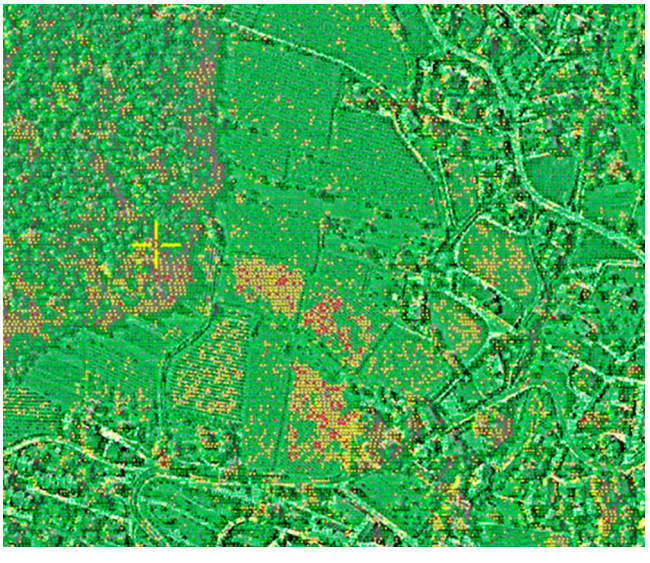

Figure 3. Homologous points of a stereo image matching case of FORSAT. The very dense green points are successfully matched points, the yellow points are still acceptable but with low reliability, and the red points are the outliers to be excluded. Note that the colours are grayscale in the print version.

Rosenholm and Torlegard 1988; Mitchell and Chadwick 1999; Beyer, Alexandrov, and Moratto 2014; Sedaghat and Naeini 2018) and is based on the estimation of the transformation parameters between two DEM patches, by minimising the sum of the squares of the elevation differences (1D along the z-axes). Nevertheless, one drawback of the approach is that the 1D elevation differences may not truly represent the surface-to-surface distance, in case of comparisons between landscape models in complex scenarios. Assuming a reference DEM and a test DEM to be checked, the above-mentioned approach based on elevation differences is suboptimal (Gruen, Poli, and Zhang 2004), since:

a) at surface discontinuities (i.e. steps) interpolation errors may lead to large height differences although the measurements are correct (Figure 4(a)), and
b) if the reference frames of the two DEMs are not perfectly aligned (e.g. shifts and tilts), then large differences occur, especially at discontinuities, although the heights may be correct in the single surfaces (Figure 4(b)).

In FORSAT, these shortcomings are overcome by employing an advanced approach where the shortest 3D (Euclidean) distance, instead of the elevation difference, between each reference point and the produced DEM is used (Gruen and Akca 2005; Akca 2010; Akca et al. 2010).

FORSAT uses the least squares 3D surface matching (LS3D) method (Gruen and Akca 2005; Akca 2007; Akca and Gruen 2007) that favourably responds to the following aspects:

1) co-registration capability with higher order spatial transformation models,
2) co-registration and comparison of full 3D surfaces (as opposed to 2.5D),
3) a rigorous mathematical formulation for high accuracy and quality control demands,
4) a flexible model for further algorithmic extensions,
5) mechanisms and statistical tools for internal quality control,
6) the capability of datasets matching at different qualities and resolutions.

The LS3D method is a rigorous algorithm for the matching of overlapping 3D surfaces and/or point clouds. It estimates the transformation parameters of one or more fully 3D surfaces with respect to a template surface, using the generalised Gauss–Markov model, minimising the sum of the squares of the Euclidean distances between the surfaces. This formulation gives the opportunity to match arbitrarily oriented 3D surfaces, without using explicit tie points. Details of the procedure can be found in Akca and Gruen (2005, 2007), together with several applications ranging from 3D modelling (Akca et al. 2007) to geomorphology (Akca and Seybold 2016).

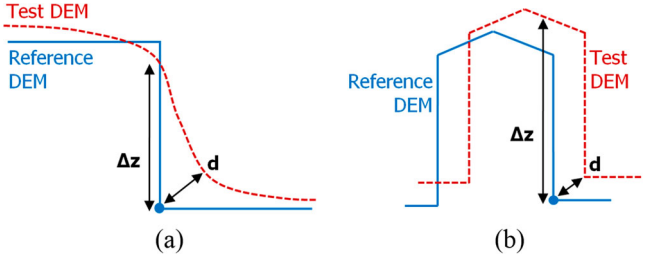

Figure 4. The sub-optimality between 1D elevation difference Δz and the spatial distance d in case of (a) surface discontinuity and (b) reference frame misalignment.

In FORSAT, the workflow for 3D comparison and change analysis includes three main steps. In the first step, the LS3D algorithm is run only one iteration, without applying any 3D transformation, in order to estimate the 3D spatial (Euclidean) distances between the DSMs. This step is very important because it gives quantitative and precise information on the initial (spatial) disagreement of the two datasets, which is caused by variant geo-referencing accuracy of each data set and temporal changes that might have occurred between the two epochs.

The second step is the surface co-registration. A full LS3D surface matching is performed to estimate any translational, rotational and scale difference between the template (fixed) and search (floating) DSMs. Then, the estimated 3D transformation parameters are applied to the search DSM and the geo-referencing errors (shown hypothetically in Figure 4(b) are eliminated.

The software provides statistical information that is helpful for in-depth analysis of the results: the a-posteriori variance factor gives information about the overall agreement of both DSMs, while the standard deviations of the estimated transformation parameters and the correlations between themselves give information concerning the stability of the system and the quality of the data content. In the course of iterations, a simple weighting scheme adapted from the robust estimation methods is used for error detection in correspondences (Gruen and Akca 2005; Akca 2010; Akca et al. 2010). Every residual is tested against a threshold that is calculated as three times of the current a posteriori standard deviation of the observations (sigma naught). In this way, the changed parts are excluded from the parameter estimation. Because of the high redundancy of a typical data set, a certain number of missed outliers, i.e. Type-II (omission) errors, do not have a significant effect on the estimated transformation parameters.

The third and final step of the 3D surface comparison is for analysis purposes. The LS3D is run again without any 3D transformation calculation, in order to compute the 3D correspondences. The 3D correspondences are vectors showing the 3D spatial deviations (or changes) between the DSMs. They are the actual change indices, and they assert the search DSM at every data point location of the template DSM. This final step shows the temporal changes of the forest surface in the form of 3D correspondence vectors.

In case of forest applications, any spatial deviation larger than ±3 m between the template and the search DSMs is classified as a temporal change, while spatial deviations less than ±3 m are labelled as 'no change' class. This number is the mean a priori accuracy of the used DSMs according to our internal tests. In fact, the mean DSM generation accuracy of the FORSAT system is about 2–3 times of the ground sampling distance (GSD) of the used imagery (Gruen, Poli, and Zhang 2004). Any spatial deviation larger than ±20 m is regarded as the gross error, excluded from the computation, labelled as 'no data', but kept in the visualisations (Figures 8, 15 and 21). These gross errors are generally due to image matching, triangulation and reconstruction problems. Their percentage is small and usually about or below 1% as seen in Figures 12, 18 and 24. When the change hypotheses are tested, two types of errors can occur in the detection results. The gross errors, whose spatial deviations are less than ±20 m, are false positively accepted, which bring Type-I (commission) errors, although they do not belong to change class in reality. On the other hand, temporal changes, whose spatial deviations are just as ±3 m or less, are false negatively rejected, which bring Type-II (omission) errors, although they belong to change class in reality. The selection of the threshold values as less than or greater than ±20 and ±3 m will accordingly change the number of Type-I and Type-II errors, respectively. These threshold values do not apply to all kind of forest types. They should be tuned according to the application site. The selection of the threshold is also correlated with the accuracy of the DSM (Qin, Tian, and Reinartz 2016).

The adopted change detection strategy is straightforward and practical. Further developments are possible to improve the error handling capacity (Wheaton et al. 2010; Lague, Brodu, and Leroux 2013).

2.7. Precision of 3D (volume) change numbers

FORSAT provides precision metrics of the estimated 3D volume change. The theoretical precision of the volumetric change value is computed from the internal (a priori) data following the law of error propagation.

Given that the volume V of any polygon with a 3D change is computed as

$$V = a \sum_{i=1}^{n} h_i, \tag{1}$$

where a is the area of the unit grid cell of the template DSM ($2 \times 2 = 4$ m^2, $4 \times 4 = 16$ m^2 and $2 \times 2 = 4$ m^2 in the Austrian, Swiss and Spanish test sites, respectively), h_i are the height differences between the template and search DSMs at every grid cell location within the polygon, n is the number of grid cells coinciding in the change polygon. The theoretical precision m_v of volume V is computed using the law of error propagation.

$$m_v^2 = \left[\frac{\partial V}{\partial a}\right]^2 m_a^2 + \left[\frac{\partial V}{\partial h_1}\right]^2 m_{h1}^2 + \left[\frac{\partial V}{\partial h_2}\right]^2 m_{h2}^2 + \cdots + \left[\frac{\partial V}{\partial h_n}\right]^2 m_{hn}^2. \tag{2}$$

The a priori precision of the area of the unit grid cell m_a is supposed to be errorless, therefore $m_a = 0$. The a priori precision of the height differences are assumed to be equal, that is:

$$m_{h1}^2 = m_{h2}^2 = \cdots = m_{hn}^2 = m_h^2. \tag{3}$$

The value of m_h can be computed as the root mean square error (RMSE) of the co-registration of small surface patches of the DSMs over flat areas. It corresponds to the uncertainty of surface match at the grid cell level. Then, Equation (2) becomes

$$m_v^2 = n \;\; a^2 \;\; m_h^2, \tag{4}$$

$$m_v^2 = a \;\; A \;\; m_h^2, \tag{5}$$

$$m_v = \sqrt{a \;\; A} \;\; m_h, \tag{6}$$

where $A = na$ is the area of the change polygon. The theoretical precision (standard deviation) of the volume values in Figures 13, 19 and 25 were computed using Equation (6). Relevant derivations were given in Bagnardi, Gonzales, and Hooper (2016), Parente and Pepe (2018), Avian, Kellerer-Pirklbauer, and Lieb (2018), Li et al. (2018), Scaioni et al. (2018) and Morino et al. (2018).

2.8. FORSAT software

The above described functionality was implemented as the software suite FORSAT using C/C++ programming language. The software suite is not a monolithic system; every core module works independently and is related to the others at the same time. The block diagram is given in Figure 5. The process starts with the metadata reading and internal format conversion. Radiometric pre-processing and pyramid generation is performed for each scene individually. If a few GCPs are available, geo-referencing accuracy can be improved by use of the RPC triangulation. Quasi-epipolar images are generated and sent to the image matching module for DSM generation. DSMs of different dates (together with external LiDAR point clouds, if available) are input to the co-registration module. Once they are accurately aligned, 3D comparison and final change analysis steps are performed.

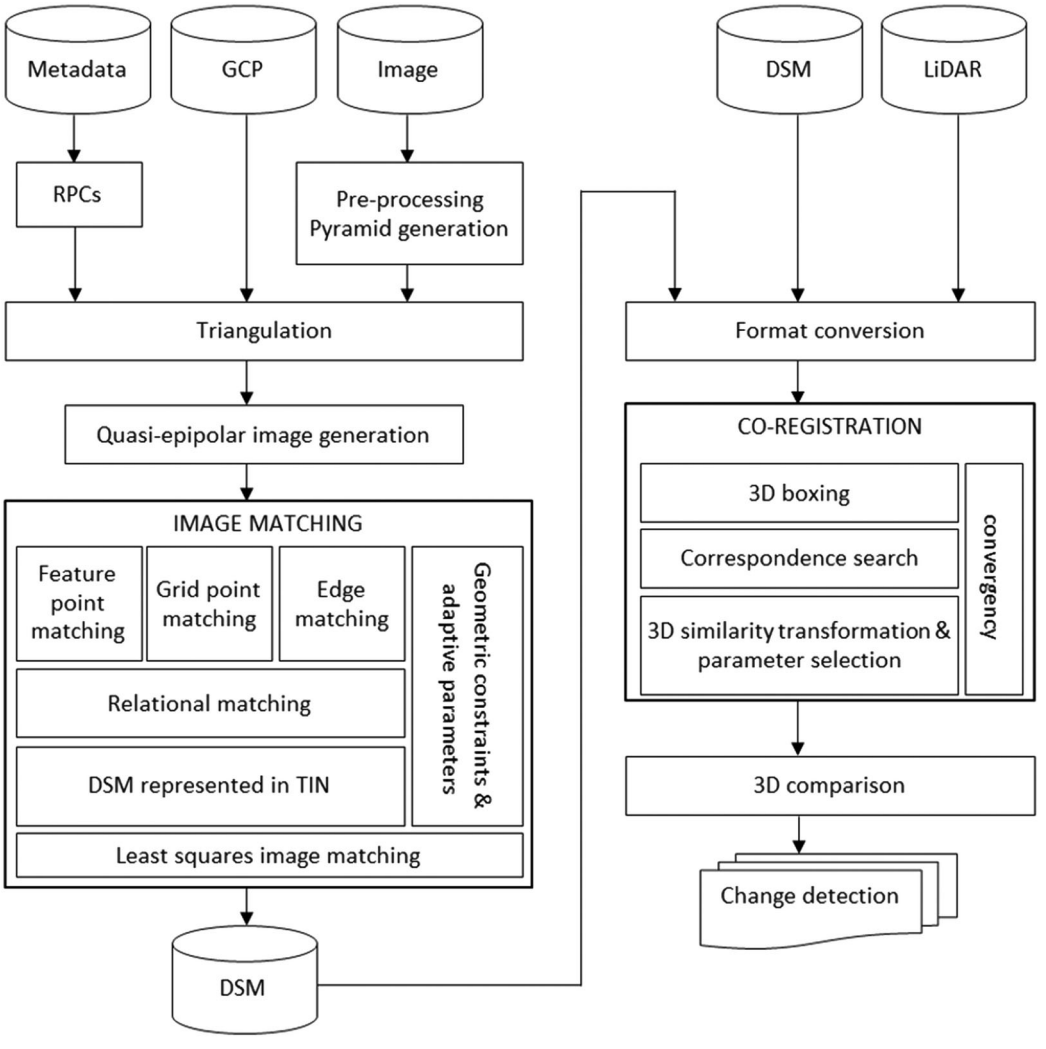

Figure 5. Block diagram of the functional modules of the FORSAT software.

3. Applications: test sites and validation

Applications and validation studies were carried out at three test sites located in Austria, Switzerland and Spain (Figure 6), using VHR satellite imagery either ordered as a new acquisition or retrieved from the archive. Pre-processing, DSM generation, co-registration and change analysis steps were performed consecutively. Accuracy evaluation was carried out only in the Austrian test site since the reference data was not available in the other test sites.

3.1. Forest damage caused by storms and pests in Salzburg (Austria)

Austria's forests cover an area of around 40,000 km^2, which is almost half the area of the whole country. This is equivalent to more than one billion cubic metres of growing wood with rich biodiversity. The wet moderate climate of Austria, which varies throughout the country, underlies intense influences from the mountainous regions and the presence of strong winds in the Austrian Alps. These heavy wind gusts cause natural hazards which also influence the forest regions. Furthermore,

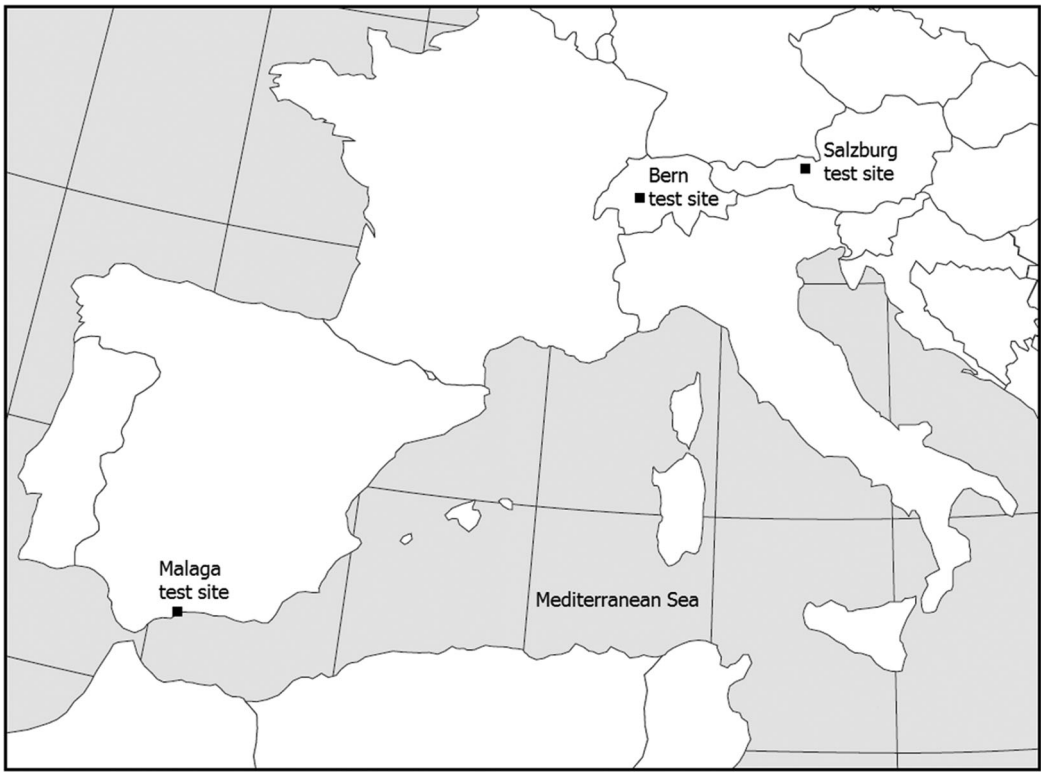

Figure 6. The three test sites in Austria, Switzerland and Spain.

Austrian forests are endangered by bark beetles which damage forest stands and the economy. Long-term projections indicate that the climate change will cause raising temperatures in Central Europe and subsequently will trigger the spread of the bark beetles at higher altitudes (Bale et al. 2002).

The test site covers an area of 100 km². It is located in the Austrian Alps near Zell am See in the province of Salzburg (Figure 6). With exception of the city of Zell am See in the South-East of the

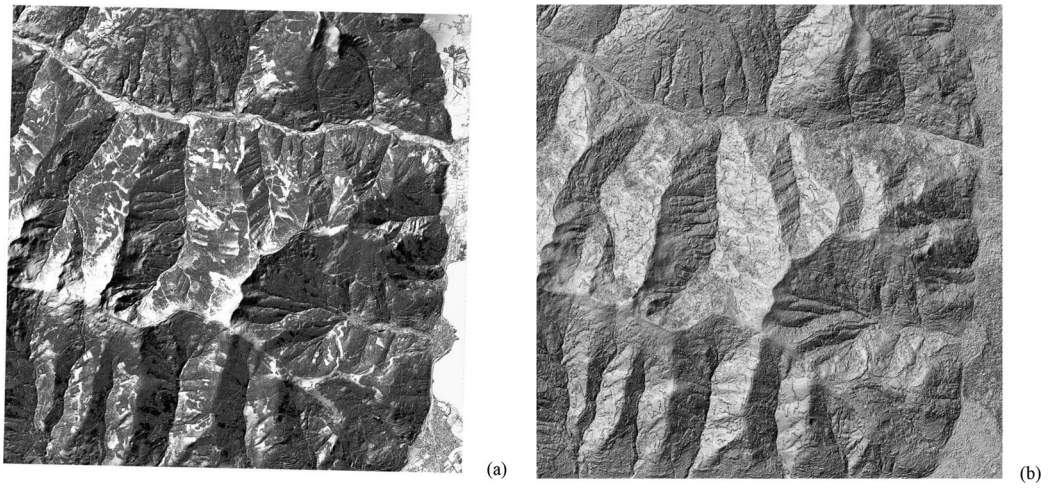

Figure 7. Historic LiDAR DSM of 2007 (a), and recent SPOT-6 DSM of 2013 (b).

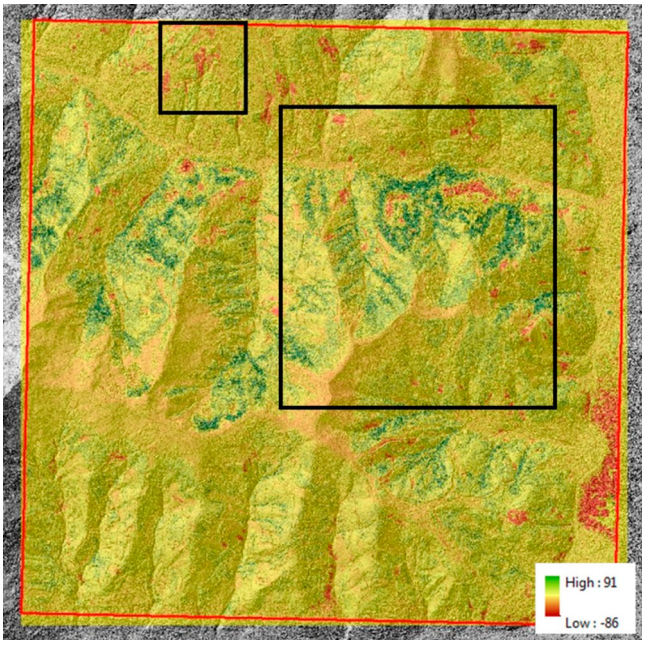

Figure 8. Result of the change analysis. The legend at the lower right corner shows the height variations between 2007 and 2013. The red colour shows the decrease of height and the green colour shows the increase of height. The colour scale is also for the Figures 9 and 10. Note that the colours are grayscale in the print version.

area of interest (AOI), the area is dominated by mountainous landscape with large forest areas. The site was damaged by storms (since 2002) and bark beetles (since 2010). As a consequence affected regions are characterised by forest clearings, which developed through the years 2002–2011.

A DSM, acquired using the airborne LiDAR scanner in 2007 and resampled to 2 m resolution was provided by the Department of Forest to be used as the historical reference data (Figure 7(a)). A new Pléiades stereo image acquisition task was ordered to be used as the recent data. Although several attempts have been made between July and August 2014, cloud–free images could not be acquired. Therefore, an archived SPOT-6 triplet from October 2013 with a resolution of 1.5 m was used as recent data. The imagery was processed using the FORSAT software, and a DSM with a resolution of 2 m was generated (Figure 7(b)).

The historic and actual DSMs were automatically co-registered and compared for 3D change detection. The red areas in Figure 8 show the decrease and the green areas show the increase in height. In Figure 9, an area of deforestation is clearly visible in the SPOT-6 true colour composite image and in the corresponding historic LiDAR and recent SPOT-6 DSMs. Due to the unfavourable acquisition time of the SPOT-6 stereo pair, large areas of the test site are covered with mountain shadows because of the low sun angle which leads to matching problems during the DSM processing and subsequently also contaminates the change results (Figure 10). This is not a specific problem to the FORSAT, rather it is a general problem of image matching algorithms using the satellite images. Selection of a better image acquisition time or employing a shadow elimination algorithm (Mostafa 2017) can resolve the problem.

The forest development plan (Figure 11) of the test area is obtained from SAGIS (Salzburger Geographisches Informationssystem) and overlaid with the change detection results so that the spatial changes in specific forest types can be identified. The protection forest (class 101) and commercial timberland (class 104) areas dominate in the test site with areal percentages of 54.3% and 38.5%, respectively (Table 1). All forest classes have a similar trend in terms of change in coverage (Figure 12). For example, 82.8% of the entire commercial timberland coverage does not show any

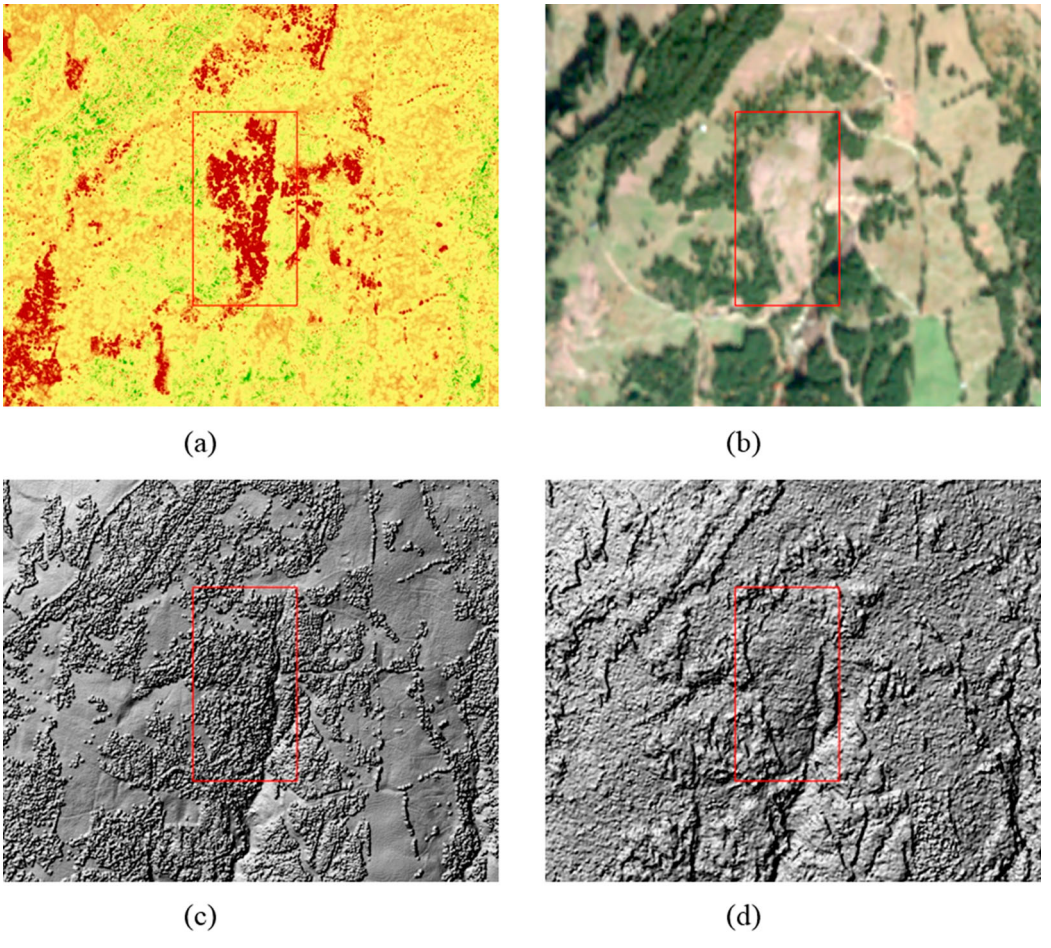

Figure 9. Enlarged view of the top-left (small) rectangle in Figure 8. Deforestation detected in the change analysis (a), SPOT-6 true colour view of the same area (b), historic LiDAR DSM (c), and recent SPOT-6 DSM (d).

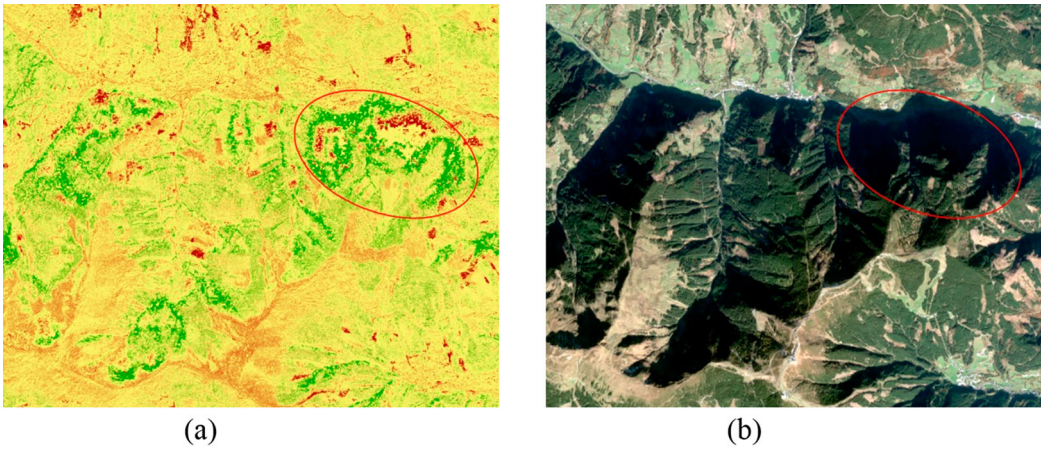

Figure 10. Enlarged view of the middle-right (large) rectangle in Figure 8. Erroneous image matching causes errors in the change detection (a), mountain shadows visible on the SPOT-6 orthoimage of the same area (b).

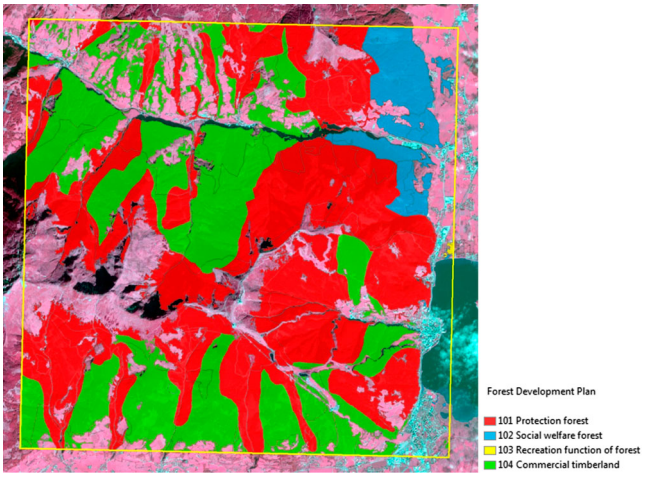

Figure 11. The forest development plan of the Salzburg test site. The background is the SPOT-6 false colour composite image.

Table 1. Percentage of the forest development plan classes in the Salzburg test site (Austria).

Class no	Land cover name	Area percentage
101	Protection forest	54.3%
102	Social welfare forest	7.2%
103	Recreation function of forest	0.1%
104	Commercial timberland	38.5%

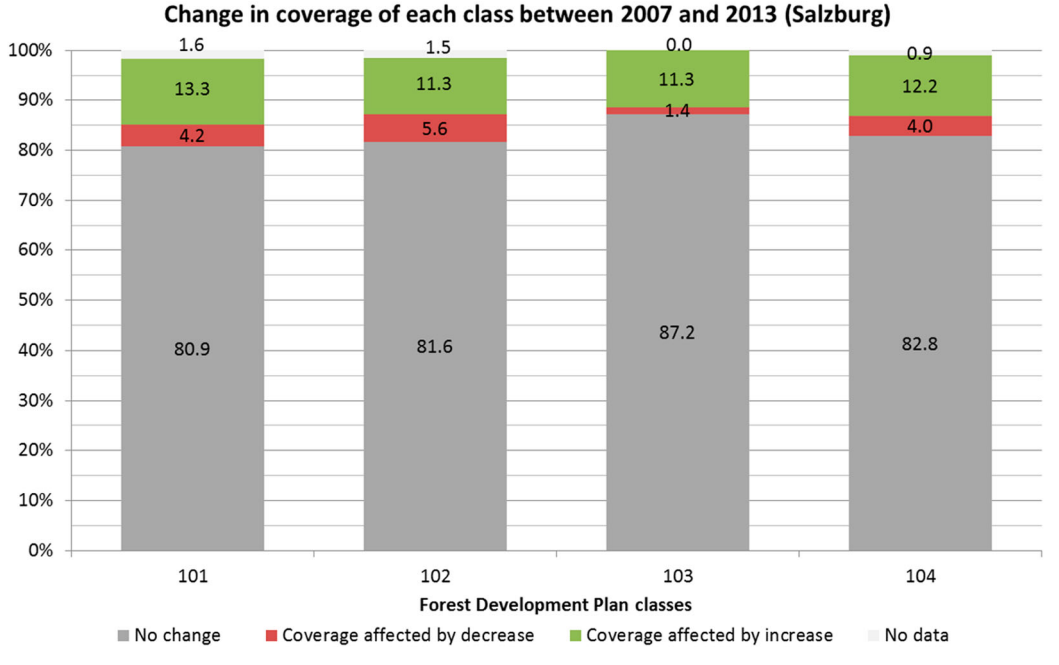

Figure 12. Areal change of each forest class coverage in the Salzburg test site.

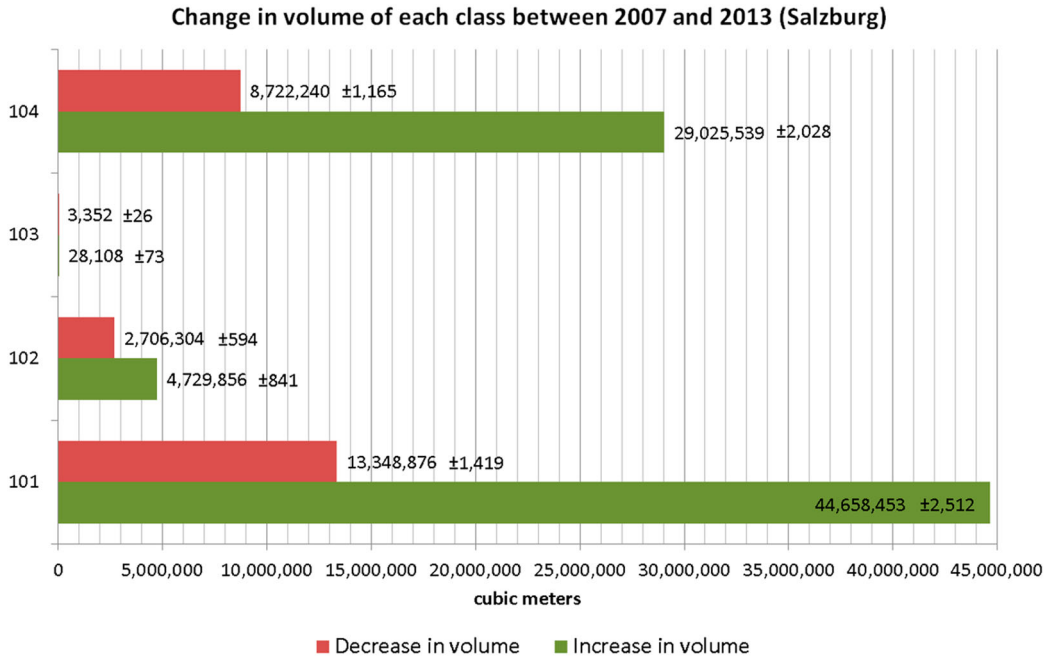

Figure 13. Volumetric change of each forest class in the Salzburg test site.

change in height between 2007 and 2013. The remaining 12.2% and 4.0% of the entire coverage increased and decreased in height, respectively. Overall, we observe an increasing trend in commercial timberland stocks in the test area.

Since the FORSAT methodology is fully 3D, a volumetric comparison provides much more valuable information. Figure 13 shows the volumetric changes of each forest class given in cubic metre. The largest change occurs in the protection forests (class 101). It lost a volume of 13.3 million m^3 due to forest clearing, whereas it gained a volume of 44.6 million m^3 due to growth, with standard deviations of ± 1419 and ± 2512 m^3, respectively.

For the validation of the change results, 60 sample points were selected in the detected deforestation class aiming to include one point per class fragment. Moreover, 140 sample points were selected in the detected non-deforestation class covering the spatial extend as randomly as possible. In both cases, the sample points were manually picked. Their actual states were manually investigated on the available (external) aerial and satellite images. The results show that the deforestation class has the correctness and completeness values of 65.0% and 73.6%, respectively. Correctness is here defined as the percentage of truly detected classes in the sample points, also referred to as user's accuracy, and is relevant to the Type-I (commission) errors. Completeness is the percentage of truly detected classes in the reference points, also referred to producer's accuracy (Heipke et al. 1997; Shufelt 1999; McKeown et al. 2000; Foody 2002; Rutzinger, Rottensteiner, and Pfeifer 2009). It is relevant to the Type-II (omission) errors.

3.2. Shrub/tree cover mapping and change detection in Bern (Switzerland)

From a climatic point of view, Switzerland can be divided into two different parts: the northern part of the Alps underlies the temperate Central European climate with stronger winters and more precipitation than the southern part, which is more influenced by the Mediterranean climate. The temperatures can vary enormously throughout the season, especially because of the extreme differences in

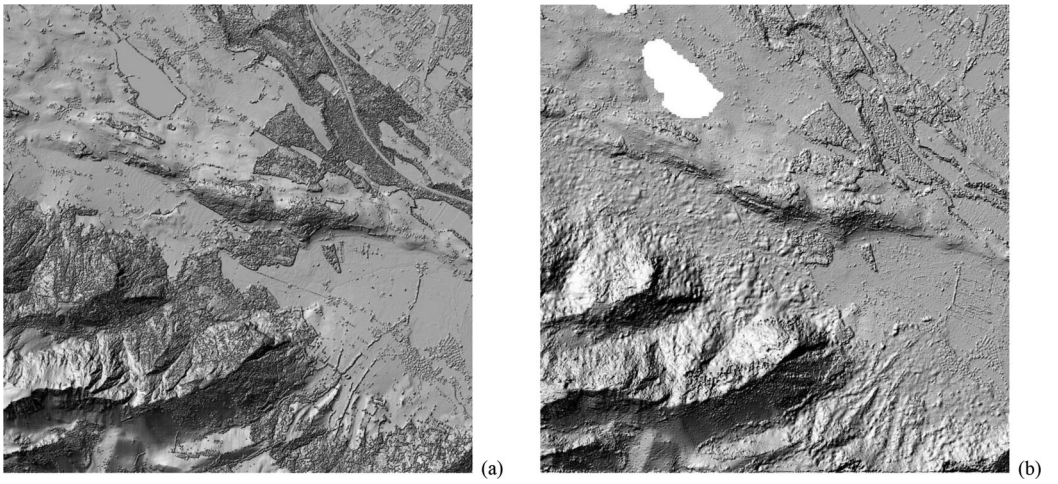

Figure 14. LiDAR DSM from 2000 (a), and IKONOS stereo imagery derived DSM from 2003 (b). Both DSMs have a resolution of 4 metres.

elevation. These diversifications can affect forests, for instance through natural hazards due to climate, and also lead to detectable changes.

The test area is near Thun in the canton of Bern (Switzerland) and covers around 27 km^2 including forestry as well as urban structures (Figure 6). It was covered by a LiDAR derived DSM from 2000 (Figure 14(a)) and IKONOS imagery derived DSM from October 2003 (Figure 14(b)). Both of the DSMs whose point spacing are 4 m, were delivered in a fashion ready for analysis (Baltsavias, Li, and Eisenbeiss 2006). The LiDAR DSM has an accuracy of 0.5 m and the IKONOS DSM about 2–

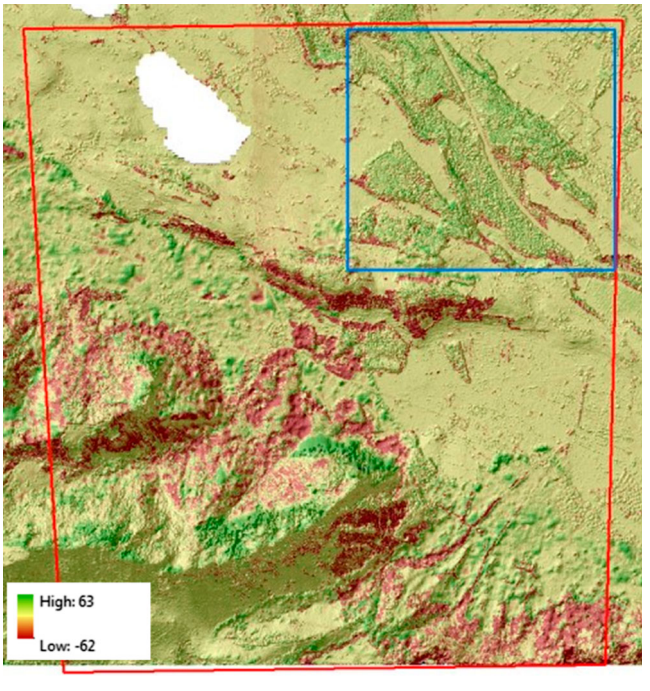

Figure 15. 3D comparison and change results of the Bern test site in Switzerland.

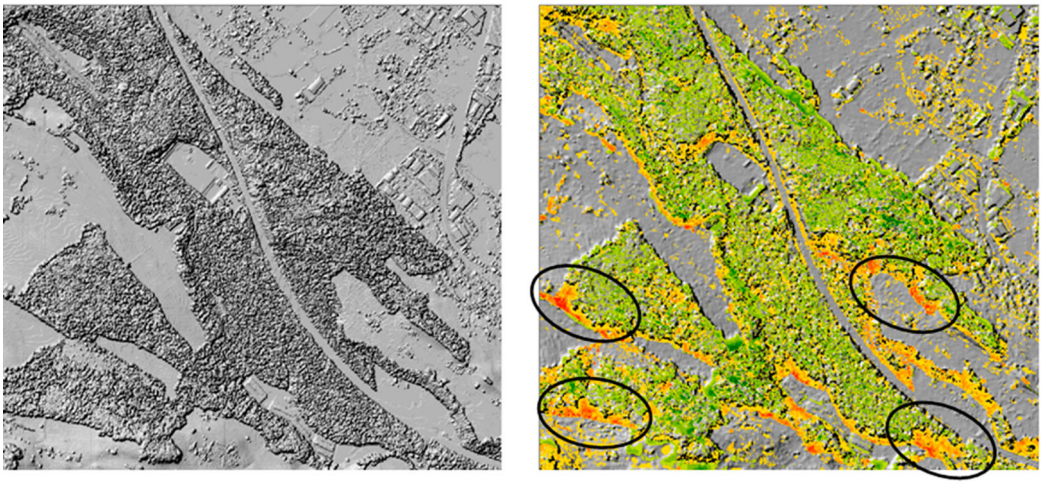

Figure 16. Enlarged view of the blue rectangle area in Figure 15. The LiDAR DSM of 2000 (a), and the IKONOS DSM together with temporal changes of 2003 (b). The black ellipsoids indicate the significant deforestation areas. Note that the colours are grayscale in the print version.

3 m. Apart from the other test site applications, where the full processing chain of the FORSAT was performed, in the Bern data set only the change detection step was performed, with special attention to change detection of shrub and tree coverage.

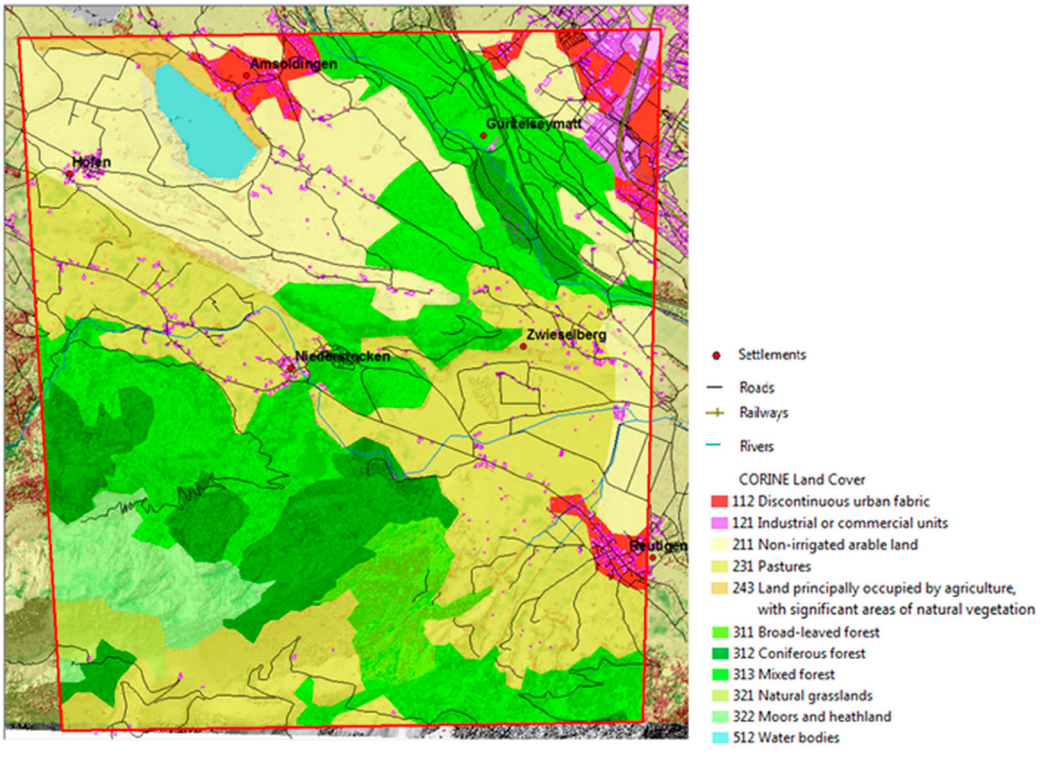

Figure 17. The CORINE land cover of the Bern test site.

Table 2. Percentage of CORINE land cover classes in the Bern test site (Switzerland).

Class no	Land cover name	Area percentage
112	Discontinuous urban fabric	4.2%
121	Industrial or commercial units	1.3%
211	Non-irrigated arable land	20.1%
231	Pastures	30.1%
243	Land principally occupied by agriculture with significant areas of natural vegetation	1.1%
311	Broad-leaved forest	3.4%
312	Coniferous forest	9.4%
313	Mixed forest	24.8%
321	Natural grasslands	1.3%
322	Moors and heathland	4.3%

The 3D Euclidean distances, showing the changes at the object surfaces, were mapped on the change layer (Figure 15). The extreme surface changes in terms of ascending and descending areas (dark green and dark red areas, respectively) in the south are due to image matching problems because of topographic effects and large shadows of the high mountains. When working with the VHR satellite imagery, special attention should be paid to the image acquisition conditions, otherwise, the image matching may fail, which ends up in geometric deformations and spikes on the reconstructed surface. Very large off-nadir angles and very low sun angles should be avoided in the new image acquisitions. Figure 16 is the enlarged view of the blue rectangle in the upper right side of Figure 15. Deforested areas, which are depicted in orange to red colour, in the outskirt regions of the forest are clearly visible (Figure 16(b)). The grey areas had not changed between 2000 and 2003. The green areas show the growth of the vegetation including the partial penetration property of LiDAR data in 2000.

The CORINE land cover layer of the year 2000 (Figure 17) was superimposed to the change layer (Figure 15). Thus, the area and volume change of each land cover class is individually determined. The pastures (class 231), mixed forest (class 313), non-irrigated arable land

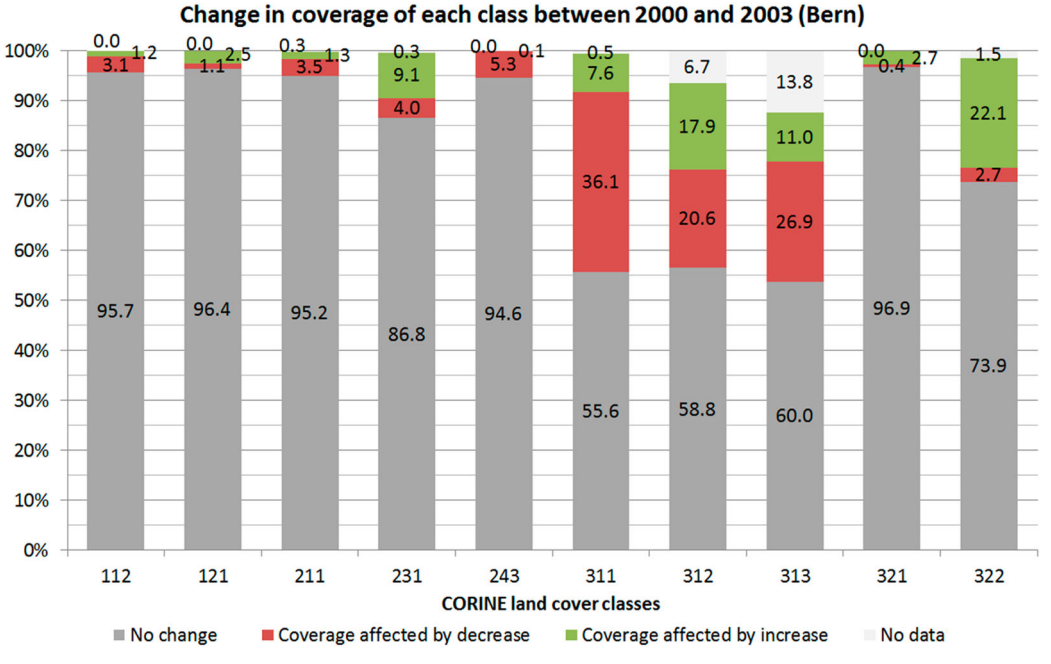

Figure 18. Areal change of each class coverage in the Bern test site.

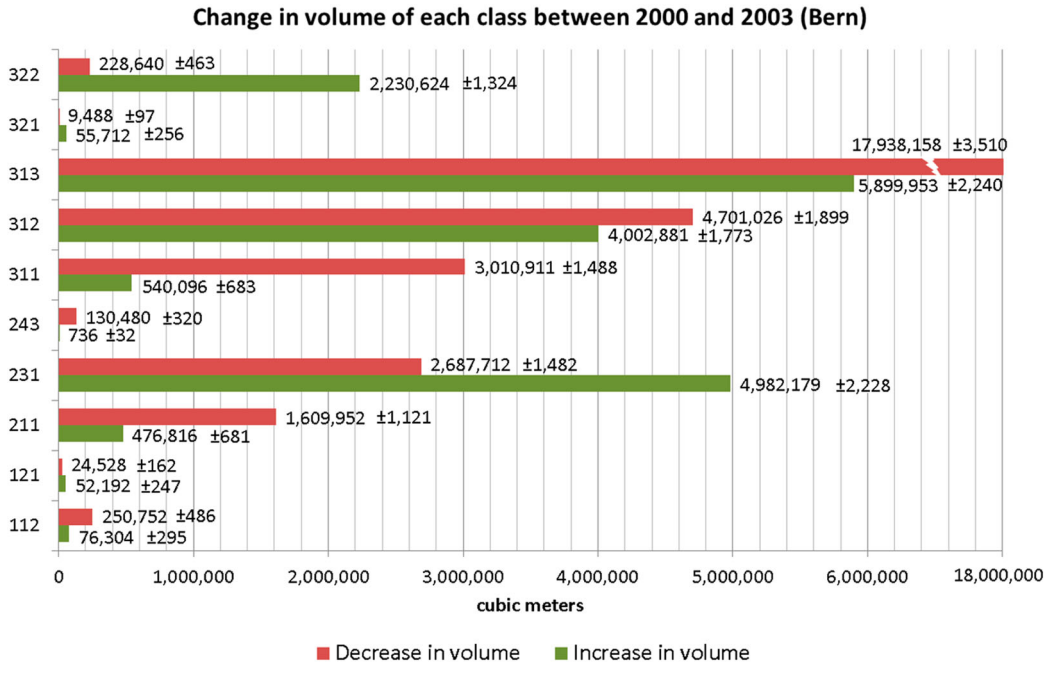

Figure 19. Volumetric change of each class in the Bern test site.

(class 211) and coniferous forest (class 312) are the dominating types of the test site (Table 2). Regarding the percentage of area affected by change, broad-leaved forest (class 311) shows the highest canopy height decrease with 36.1% followed by the mixed forests (class 313) with 26.9% and the coniferous forests (class 312) with 20.6% (Figure 18). In case of the change of increase in canopy height, the moors and heathland (class 322) with 22.1%, the coniferous forests (class 312) with 17.9% and the mixed forests (class 313) with 11.0% have the highest percentage of the affected area.

When the volumetric change is considered, different classes attracted attention. The shrub related classes 322 and 231 show a considerable increase in their volume up to 2.2 million ± 1324 m^3 and 5.0 million ± 2228 m^3, respectively (Figure 19). The mixed forest (class 313) has the greatest volume changes both along the decrease and increase sides with 17.9 million ± 3510 m^3 and 5.9 million ± 2240 m^3, respectively. Therefore, 12.0 million m^3 mixed forest stock has been lost in between 2000 and 2003.

3.3. Man-made changes in Malaga (Spain)

Economic and urban growth pressures, as well as the further expansion of infrastructures, cause considerable deforestation in Spain. An infrastructural development case, which is a highway project near Malaga, Spain, was selected as another test site to show the capabilities of the FORSAT methodology (Figure 6). The site is located in the south-west of the city of Malaga and covers about 40 km^2 of hills in the south-west and flat urban areas in the north. The development of Malaga has led to new construction of a highway 'Autovía del Mediterráneo', which has been at the expense of loss of forest and agricultural areas. The highway crosses the test site along North to South directions.

In the area several archival VHR satellite imagery acquisitions are available, thus a new image order was not required. A set of IKONOS stereo imagery from December 2003 is used as the

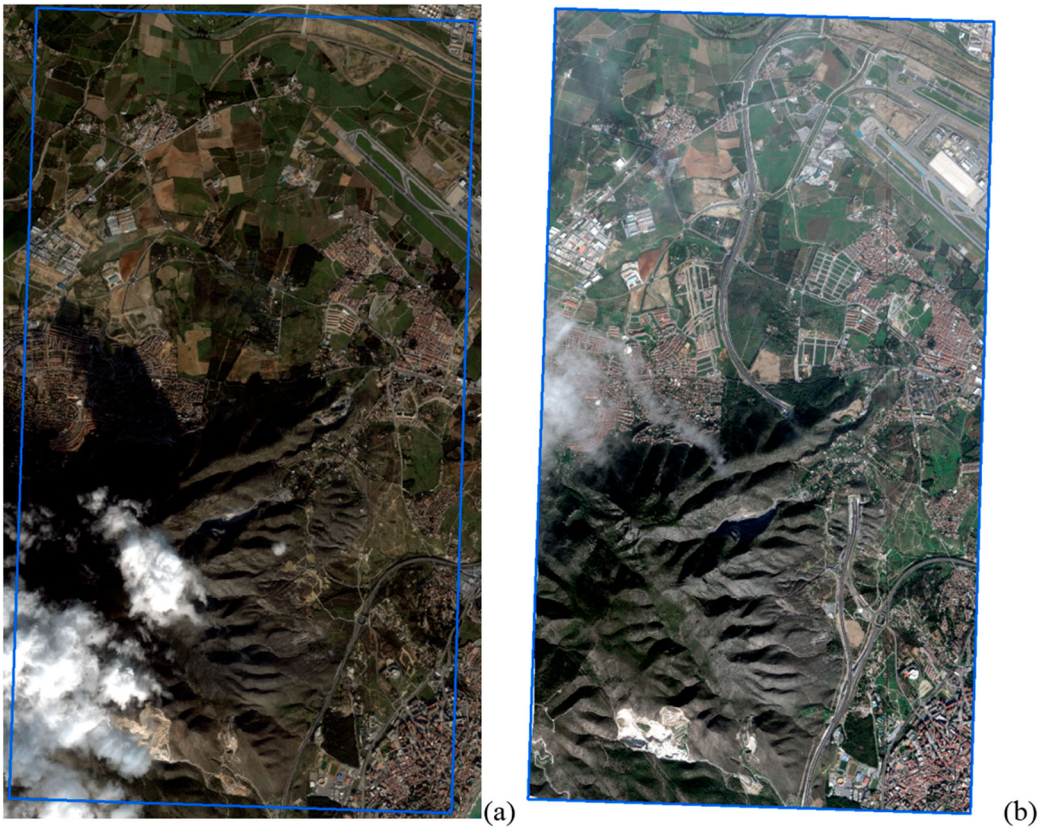

Figure 20. Input image data sets. The historical IKONOS image from December 2003 (a), and the recent Pléiades image from December 2012 (b).

historic data which depicts the surface topography in the past (Figure 20(a)). A set of Pléiades stereo imagery from December 2012 is used as the recent data which shows infrastructural developments and consequently deforestation (Figure 20(b)). Both stereo pairs have considerable areas of cloud and shadow coverage, which were masked out in the following FORSAT image matching step. The generated IKONOS and Pléiades DSMs (both in 2 m resolution) were compared in FORSAT. The resulting change layer is visualised in Figure 21 from red (decrease in height) to green (increase in height) colour. The black ellipse shows the construction of the new highway. The red linear feature below the ellipse corresponds to the border line forest cut and earthworks excavation along the previously existing highway. The enlarged view of the black rectangle in Figure 22 shows the construction of the tunnel portal and the feeder motorway. The excavations (in red colour) and embankments (in green colour) can clearly be identified along the highway route.

The land use classes in the Forest Plan Andalusia (PFA), which is shown in Figure 23, were intersected with the change layer so that each land use type is analysed individually. The test area is highly urbanised with large urban and agriculture classes whose coverages are 37.3% and 33.5%, respectively (Table 3). The largest forest class is other woody plants with 19.9% coverage, predominately located in the mountainous region.

When considering the changes of the canopy coverage, the olive trees (class 70) are the most changed with an increase in height of 47.8% of its area and a decrease in height of 16.6%. Note that the olive trees class has the smallest class coverage with 0.01% in the whole test area

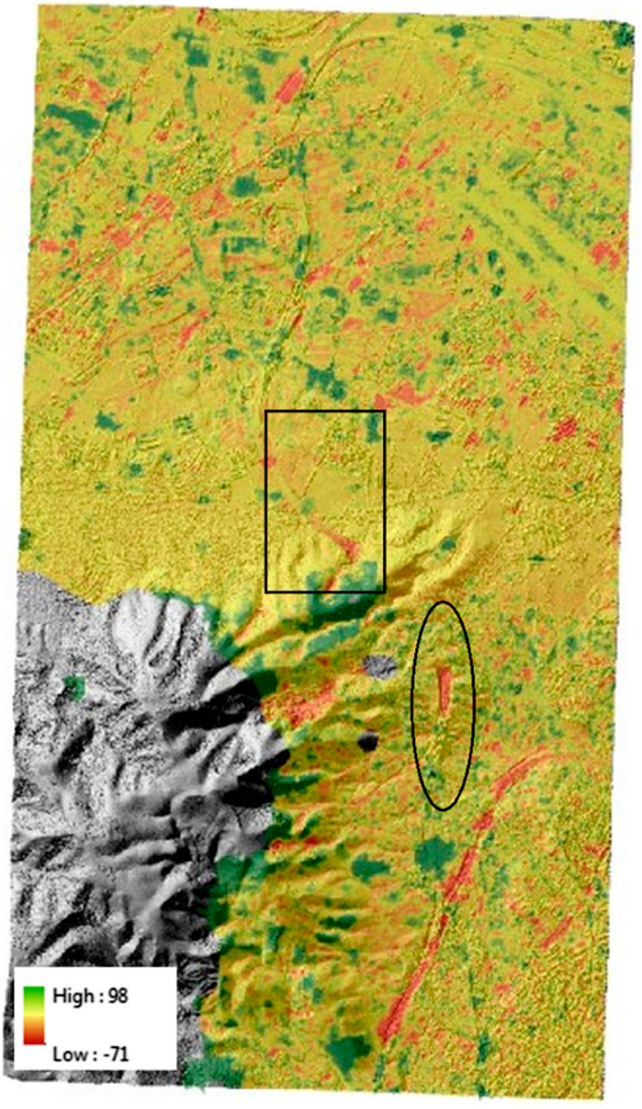

Figure 21. Change results of the Malaga test site. The enlarged view of the black rectangle is given in Figure 22. Note that the colours are grayscale in the print version.

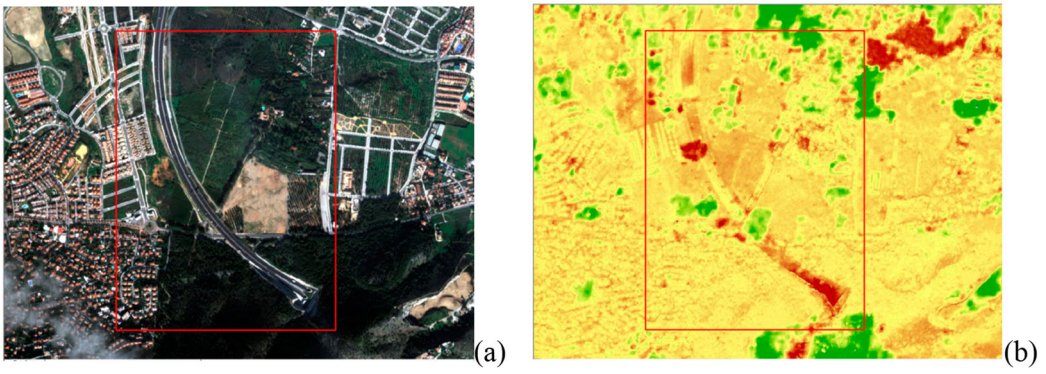

Figure 22. Enlarged view of the black rectangle in Figure 21. Pléiades true colour composite (a), and change layer of the corresponding coverage (b). Note that the colours are grayscale in the print version.

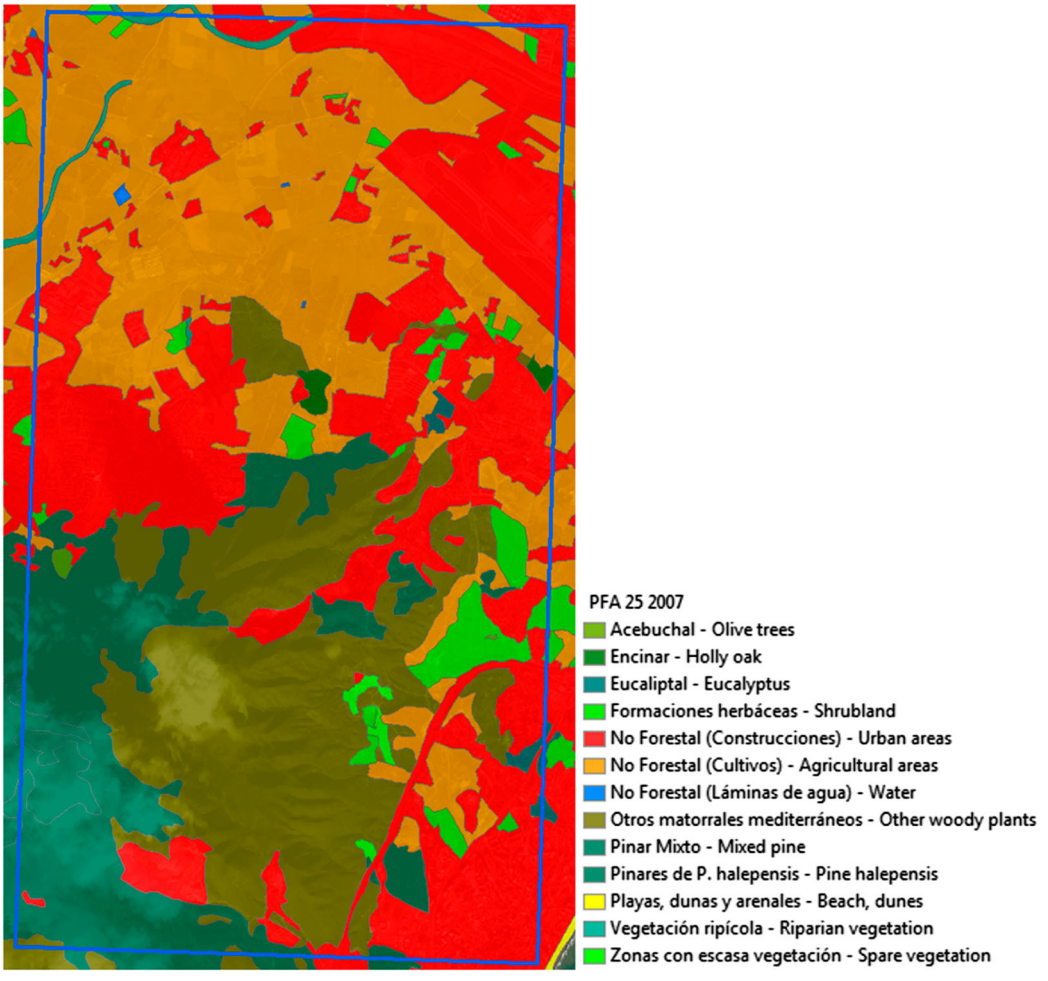

Figure 23. Land use types of the Forest Plan Andalusia of the Malaga test site.

(Figure 24). This diagram also shows that the classes with a large percentage of changes like other woody plants (class 130) and spare vegetation (class 180) are located in the vicinity of the route of the new highway.

Table 3. Percentage of the land cover classes of the Forest Plan Andalusia in the Malaga test site (Spain).

Class no	Land cover name	Area percentage
20	Holly oak	0.4%
70	Olive trees	0.1%
80	Eucalyptus	0.4%
103	Pine halepensis	4.0%
130	Other woody plants	19.9%
140	Shrub	3.4%
150	Riparian vegetation	0.5%
180	Spare vegetation	0.5%
9991	Agricultural	33.5%
9992	Water	0.1%
9993	Urban	37.3%

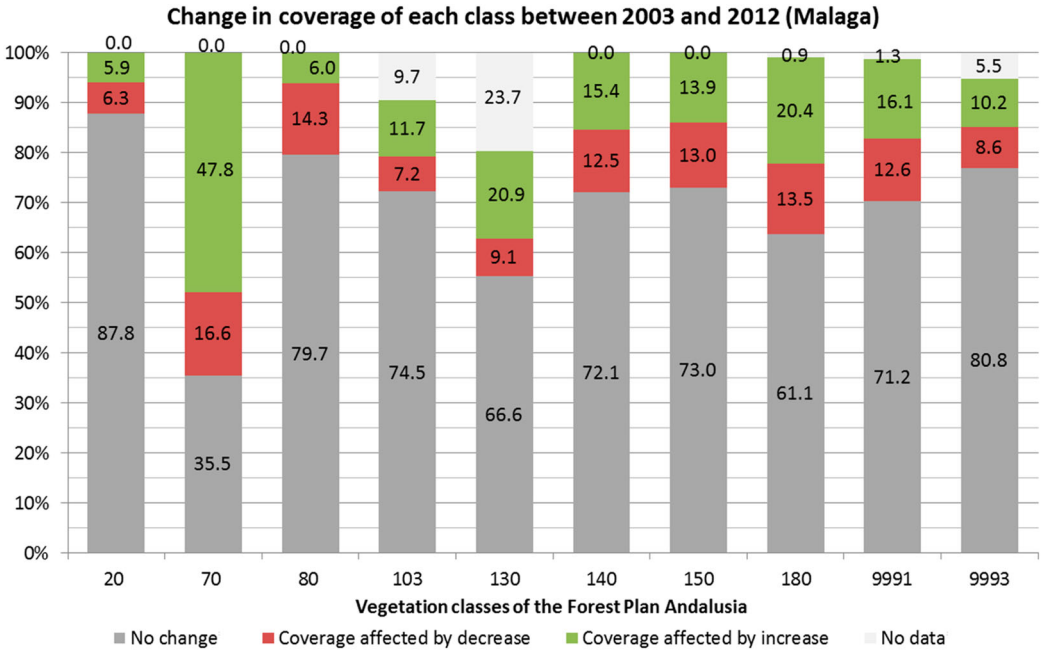

Figure 24. Areal change of each class coverage in the Malaga test site.

Regarding the changes in volume, the urban (class 9993) and agriculture (class 9991) types show large undulations both in decrease and increase directions. This is the outcome of ongoing construction and cultivation activities of the area. During the nine years of the time span, the other woody plants (class 130) lost 6.6 million ± 827 m^3 and gained 21.9 million ± 1256 m^3 in volumes (Figure 25).

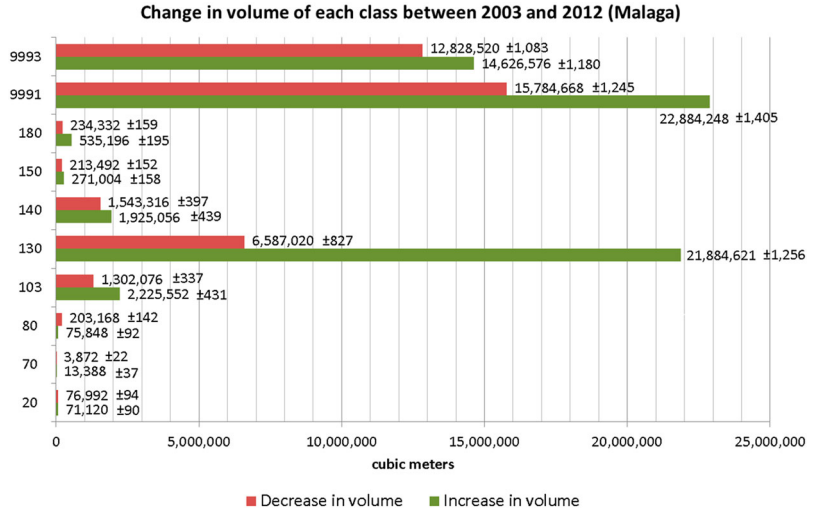

Figure 25. Volumetric change of each class in the Malaga test site.

4. Discussion

Conventionally, information related to trees, for example height, cross-section area, diameter at breast height (DBH, i.e. diameter at 1.3 m above ground) are measured in the field using several tools such as calipers, steel tapes, optical devices, level rods and hypsometers (Husch, Miller, and Beers 1982; Päivinen, Nousiainen, and Korhonen 1992; Korhonen et al. 2006). Collecting forest information through ground/field measurements is slow and expensive (Pouliot et al. 2002). All around the world, forests are becoming more and more vulnerable to fires, droughts, insect epidemic, and diseases because of climate change (Foley et al. 2005). The increasing demands for rapid, up-to-date and comprehensive information led to more effective solutions. Remote sensing-based techniques offer such effective tools for monitoring and evaluating forest treatments (Noujdina and Ustin 2008; Ke, Quachenbush, and Im 2010; Van Leeuwen and Nieuwenhuis 2010).

FORSAT is a 3D forest information solution using VHR satellite imagery as the primary data source. It is a complete system offering the full steps of the processing chain from pre-processing and image orientation to DSM generation and change analysis. It provides quick and on-instant forest change information in area and volume dimensions. It is a unique system providing volumetric changes and their error bounds. On the other hand, it is a straightforward method which does not take into account the surface roughness, image texture, and spectral information. It also includes inherent limitations such as the difference between timber volumes and crown volumes or seasonal effects due to changes in the leaf area in non-evergreen forests.

Increasing usage of remote sensing data and methods in forestry led to develop software and tools. Examples are the forest vitality and change monitoring (FVCM) tool (Marx and Tetteh 2017), CLASlite software (Asner et al. 2009) and high resolution inventory solutions (HRIS) system (Sambatti et al. 2017). They perform general tasks as image registration, classification, disturbance monitoring and 2D mapping. They have input data restrictions, such that HRIS uses LiDAR, colour infrared and ground sampling; FVCM uses only RapidEye data, while CLASlite uses data only from Landsat, SPOT, Terra and Aqua satellites. FORSAT differs in the sense that it is a single purpose (deforestation and change detection) application by use of multiple sources (several VHR satellite images and LiDAR point clouds if available) data. It has 3D capabilities with embedded image matching module for DSM generation and a surface matching module for 3D volumetric change detection. Below are the key features which altogether make FORSAT a viable option over the alternatives.

1) Input of triplet and stereo VHR satellite images,
2) RPC block adjustment for improvement of the geo-positioning accuracy,
3) An advanced multi-image matching algorithm,
4) Coarse-to-fine hierarchical image matching capability,
5) Epipolar constrained image matching in order to reduce the correspondence search space,
6) Hybrid image matching by a combination of area-based and feature-based methods,
7) Refined point matching by use of the multi-photo geometrically constrained matching (Gruen and Baltsavias 1988),
8) Dense image matching output,
9) Genuine 3D co-registration and surface matching method for accurate DSM alignment,
10) Theoretical precision of the estimated 3D transformation parameters and statistical tools for internal quality control,
11) The capability of matching of surface datasets from different sources and at different qualities and resolutions,
12) 3D change detection which can be factorised into vertical, horizontal and volume dimensions,
13) The capability of computation of the 3D volume of changes together with theoretical precisions,
14) Standalone software implementation in which all required libraries and functions are owned and embedded.

FORSAT software requires at least a 4 GB memory (higher is preferred), a fast CPU and a high performance graphic card. Computational burden is heavy. It takes 6–8 h of time from pre-processing to end results for a moderate size forest (such as the Salzburg data set).

FORSAT software is more efficient where two or more VHR image derived DSMs are compared. It can also handle the mixed case where one of them is a LiDAR derived DSM. This is a matter of data availability, although it is not a favourable situation, since the LiDAR DSM will be systematically lower due to vegetation penetration (Matikainen, Hyyppa, and Kaartinen 2009; Ressl et al. 2016; Simpson, Smith, and Wooster 2017). The penetration ability changes with the flying altitude and pulse repetition frequency (Lee and Wang 2018). Moreover, LiDAR scan angle can be off-nadir and highly variable in the same flight strip or across different flight strips, which causes modelling problems along the canopy surface (Liu et al. 2018).

If FORSAT is to be used in a different type of ecosystem, for example monitoring a pest impact on a corn plantation, the image resolution (accordingly the DSM resolution) and threshold values should be set appropriately. Prospective applications could be individual tree detection, carbon estimation, forest fire severity analysis, monitoring of clearing, logging and other forest disturbances. When only a few trees (or a large number of trees in total, but from irregular locations within the study area) are missed or removed, change detection may fail, since such cartographic details cannot be delineated with the current resolution levels of the VHR satellite images. Processing of the GEDI (Global Ecosystem Dynamics Investigation) data is another possible application. GEDI is a LiDAR sensor that was mounted on the International Space Station (ISS) in late 2018 with the primary mission being the 3D mapping of the world's forests. GEDI is the first spaceborne LiDAR, which will possibly open new doors in the realm of 3D forest modelling.

5. Conclusions

Quick and economical ways of detecting of planimetric and volumetric changes of forest areas are desirable. Our FORSAT, an operational system, is capable of providing such spatial information for long-term monitoring of forest areas. The implemented methodology allows analysing raw satellite imagery and extracting meaningful and quantitative information about the world's forests, such as area, volume and measurements of deforestation of a forest.

The basic input data is the VHR optical satellite imagery from various sensors. The processing chain is a thorough methodology, which was implemented under a single, universal and compact software solution. Image data from multiple satellite sensors are input to single-source software, therefore a standard change output can be generated. The three pilot applications with different objectives demonstrate the capability and replicability of the FORSAT methodology. The basic forest deforestation causes such as storms, pests, fires, shrub/tree coverage degenerations, urbanisation and infrastructural construction activities can be detected and quantified. Not only 2D area computations but also 3D volume computations can be performed so that the change in the forest stocks can be analysed. A rigorous evaluation on uncertainties of volume measurements is provided in the form of theoretical precisions.

Resulting change analysis provides an insight into the space–time evolution of forests, and allows various service applications related to forest industry as well as other topics such as urbanisation, construction, agriculture, geomorphology, mining, etc. The results have generated recommendations for the public bodies and private organisations to use VHR satellite data for many forest information needs, which do not require centimetre accuracy. The presented FORSAT system is an affordable and reliable solution for sustainable forest management. It is a unique supplementing software for enhancing current forest operations.

Acknowledgements

We thank the anonymous reviewers for their valuable comments. Their contribution improved the quality of the manuscript.

Disclosure statement

No potential conflict of interest was reported by the authors.

Funding

This research received funding from the EUROSTARS [grant number E!7358] funding scheme, co-funded by the European Commission and the participating countries.

ORCID

Efstratios Stylianidis http://orcid.org/0000-0002-0188-5117
Devrim Akca http://orcid.org/0000-0002-1510-8677

References

Ackermann, F., and M. Hahn. 1991. "Image Pyramids for Digital Photogrammetry." In *Digital Photogrammetric Systems*, edited by Ebner, Fritsch, and Heipke, 43–58. Karlsruhe: Wichmann.

Akca, D. 2007. "Least Squares 3D Surface Matching". Ph.D. thesis, Institute of Geodesy and Photogrammetry, ETH Zurich, Switzerland. Mitteilungen Nr.92, 78 pages.

Akca, D. 2010. "Co-registration of Surfaces by 3D Least Squares Matching." *Photogrammetric Engineering and Remote Sensing* 76 (3): 307–318. doi:10.14358/PERS.76.3.307.

Akca, D., M. Freeman, I. Sargent, and A. Gruen. 2010. "Quality Assessment of 3D Building Data." *The Photogrammetric Record* 25 (132): 339–355. doi: 10.1111/j.1477-9730.2010.00598.x.

Akca, D., and A. Gruen. 2005. "Recent Advances in Least Squares 3D Surface Matching." In *Optical 3-D Measurement Techniques VII*. Vol. II., edited by A. Gruen and H. Kahmen, 197–206. Vienna: Wichmann. Austria, October 3-5.

Akca, D., and A. Gruen. 2007. "Generalized Least Squares Multiple 3D Surface Matching". International Archives of the Photogrammetry, Remote Sensing and Spatial Information Sciences 36(3/W52): 1-7.

Akca, D., F. Remondino, D. Novak, T. Hanusch, G. Schrotter, and A. Gruen. 2007. "Performance Evaluation of a Coded Structured Light System for Cultural Heritage Applications". Videometrics IX, Proc. of SPIE-IS\&T Electronic Imaging, San Jose (California), USA, SPIE 6491 (2007) 64910V-1-12.

Akca, D., and H. Seybold. 2016. "Monitoring of a Laboratory-Scale Inland-Delta Formation Using a Structured-Light System." *The Photogrammetric Record* 31 (154): 121–142. doi: 10.1111/phor.12149.

Asner, G. P., D. E. Knapp, A. Balaji, and G. Paez-Acosta. 2009. "Automated Mapping of Tropical Deforestation and Forest Degradation: CLASlite." *Journal of Applied Remote Sensing* 3 (033543). doi: 10.1117/1.3223675.

Avian, M., A. Kellerer-Pirklbauer, and G. K. Lieb. 2018. "Geomorphic Consequences of Rapid Deglaciation at Pasterze Glacier, Hohe Tauern Range, Austria, Between 2010 and 2013 Based on Repeated Terrestrial Laser Scanning Data." *Geomorphology* 310: 1–14.

Bagnardi, M., P. J. Gonzales, and A. Hooper. 2016. "High-Resolution Digital Elevation Model from Tri-Stereo Pleiades-1 Satellite Imagery for Lava Flow Volume Estimates at Fogo Volcano." *Geophysical Research Letters* 43: 6267–6275. doi: 10.1002/2016GL069457.

Bale, J. S., G. J. Masters, I. D. Hodkins, C. Awmack, T. M. Bezemer, V. K. Brown, J. Butterfield, et al. 2002. "Herbivory in Global Climate Change Research: Direct Effects of Rising Temperature on Insect Herbivores." *Global Change Biology* 8: 1–16.

Baltsavias, E., A. Gruen, L. Zhang, H. Eisenbeiss, and L. T. Waser. 2008. "High-Quality Image Matching and Automated Generation of 3D Tree Models." *International Journal of Remote Sensing* 29 (5): 1243–1259. doi: 10.1080/01431160701736513.

Baltsavias, E., S. Kocaman, D. Akca, and K. Wolff. 2007. "Geometric and Radiometric Investigations of Cartosat-1 Data". ISPRS Hannover Workshop 2007, "High Resolution Earth Imaging for Geospatial Information", Hannover, Germany, May 29–June 1 (on CD-ROM).

Baltsavias, E., Z. Li, and H. Eisenbeiss. 2006. "DSM Generation and Interior Orientation Determination of IKONOS Images Using a Testfield in Switzerland." *Photogrammetrie Fernerkundung Geoinformation* 2006 (1): 41–54.

Baltsavias, E., M. Pateraki, and L. Zhang. 2001. "Radiometric and Geometric Evaluation of IKONOS Geo Images and Their Use for 3D Building Modelling". In Proceedings of Joint ISPRS Workshop High Resolution Mapping from Space 2001, September 19-21, Hannover, Germany.

Baron, D., and S. Erasmi. 2017. "High Resolution Forest Maps from Interferometric TanDEM-X and Multitemporal Sentinel-1 SAR Data". *PFG – Journal of Photogrammetry. Remote Sensing and Geoinformation Science* 85: 389–405.

Beyer, R. A., O. Alexandrov, and Z. Moratto. 2014. "Aligning Terrain Model and Laser Altimeter Point Clouds with the Ames Stereo Pipeline". In: 45th Lunar Planetary Science Conference Abstracts, pp. 2902.
Broxton, M. J., and L. J. Edwards. 2008. "The Ames Stereo Pipeline: Automated 3D Surface Reconstruction from Orbital Imagery". In: 39th Lunar and Planetary Science Conference Abstracts, p. 2419.
Castillo, J. A. A., A. A. Apan, T. N. Maraseni, and S. G. Salmo III. 2017. "Estimation and Mapping of Above-Ground Biomass of Mangrove Forests and Their Replacement Land Uses in the Philippines Using Sentinel Imagery." *ISPRS Journal of Photogrammetry and Remote Sensing* 134: 70–85.
Charru, M., I. Seynave, J.-C. Herve, R. Bertrand, and J.-D. Bontemps. 2017. "Recent Growth Changes in Western European Forests Are Driven by Climate Warming and Structured Across Tree Species Climatic Habitats." *Annals of Forest Science* 74: 33. doi: 10.1007/s13595-017-0626-1.
Chen, B., X. Xiao, X. Li, L. Pan, R. Doughty, J. Ma, J. Dong, et al. 2017. "A Mangrove Forest Map of China in 2015: Analysis of Time Series Landsat 7/8 and Sentinel-1A Imagery in Google Earth Engine Cloud Computing Platform." *ISPRS Journal of Photogrammetry and Remote Sensing* 131: 104–120.
Dash, J. P., M. S. Watt, G. D. Pearse, M. Heaphy, and H. S. Dungey. 2017. "Assessing Very High Resolution UAV Imagery for Monitoring Forest Health During a Simulated Disease Outbreak." *ISPRS Journal of Photogrammetry and Remote Sensing* 131: 1–14.
Desclée, B., P. Bogaert, and P. Defourny. 2006. "Forest Change Detection by Statistical Object-Based Method." *Remote Sensing of Environment* 102 (1): 1–11.
Dial, G., and J. Grodecki. 2002. "Block Adjustment with Rational Polynomial Camera Models". In Proceedings of ACSM–ASPRS 2002 Annual Conference.
Ebner, H., and G. Strunz. 1988. "Combined Point Determination Using Digital Terrain Models as Control Information". *International Archives of Photogrammetry and Remote Sensing* 27(B11/3): 578–587.
Fankhauser, K. E., N. S. Strigul, and D. Gatziolis. 2018. "Augmentation of Traditional Forest Inventory and Airborne Laser Scanning with Unmanned Aerial Systems and Photogrammetry for Forest Monitoring." *Remote Sensing* 10: 1562. doi: 10.3390/rs10101562.
Fassett, C. I. 2016. "Ames Stereo Pipeline-Derived Digital Terrain Models of Mercury from MESSENGER Stereo Imaging." *Planetary and Space Science* 134: 19–28.
Feng, M., J. O. Sexton, C. Huang, A. Anand, S. Channan, X.-P. Song, D.-X. Song, D.-H. Kim, P. Noojipady, and J. R. Townshen. 2016. "Earth Science Data Records of Global Forest Cover and Change: Assessment of Accuracy in 1990, 2000 and 2005 Epochs." *Remote Sensing of Environment* 184: 73–85. doi: 10.1016/j.rse.2016.06.012.
Foley, J. A., R. DeFries, G. P. Asner, C. Barford, G. Bonan, S. R. Carpenter, F. S. Chapin, et al. 2005. "Global Consequences of Land use." *Science* 309 (5734): 570–574. doi: 10.1126/science.1111772.
Foody, G. M. 2002. "Status of Land Cover Classification Accuracy Assessment." *Remote Sensing of Environment* 80 (1): 185–201.
Fraser, C., E. P. Baltsavias, and A. Gruen. 2002. "Processing of IKONOS Imagery for sub-Meter 3D Positioning and Building Extraction." *ISPRS Journal of Photogrammetry and Remote Sensing* 56 (3): 177–194.
Gong, K., and D. Fritsch. 2018. "Point Cloud and Digital Surface Model Generation from High Resolution Multiple View Stereo Satellite Imagery." *The International Archives of the Photogrammetry. Remote Sensing and Spatial Information Sciences* XLII (2): 363–370. doi: 10.5194/isprs-archives-XLII-2-363-2018.
Gonzalez-Aguilera, D., L. Lopez-Fernandez, P. Rodriguez-Gonzelvez, D. Hernandez-Lopez, D. Guerrero, F. Remondino, F. Menna, et al. 2018. "GRAPHOS – Open-Source Software for Photogrammetric Applications." *The Photogrammetric Record* 33 (161): 11–29.
Grodecki, J., and G. Dial. 2003. "Block Adjustment of High-Resolution Satellite Images Described by Rational Polynomials." *Photogrammetric Engineering & Remote Sensing* 69 (1): 59–68.
Gruen, A. 2008. "Scientific-Technological Developments in Photogrammetry and Remote Sensing Between 2004 and 2008." In *Advances in Photogrammetry, Remote Sensing and Spatial Information Sciences: 2008 ISPRS Congress Book*, edited by Zhilin Li, Jun Chen, and Emmanuel Baltsavias, 21–25. London: Taylor and Francis.
Gruen, A. 2012. "Developments and Status of Image Matching in Photogrammetry." *The Photogrammetric Record* 27 (137): 36–57. doi: 10.1111/j.1477-9730.2011.00671.x.
Gruen, A., and D. Akca. 2005. "Least Squares 3D Surface and Curve Matching." *ISPRS Journal of Photogrammetry and Remote Sensing* 59 (3): 151–174. doi: 10.1016/j.isprsjprs.2005.02.006.
Gruen, A., and E. P. Baltsavias. 1988. "Geometrically Constrained Multiphoto Matching." *Photogrammetric Engineering & Remote Sensing* 54 (5): 633–641.
Gruen, A., D. Poli, and L. Zhang. 2004. "SPOT-5/HRS Stereo Images Orientation and Automated DSM Generation." *International Archives of Photogrammetry and Remote Sensing* 35 (1): 421–432.
Heipke, C., H. Mayer, C. Wiedemann, and O. Jamet. 1997. "Evaluation of Automatic Road Extraction." *International Archives of Photogrammetry and Remote Sensing* 32 (3-2W3): 47–56.
Hermosilla, T., M. A. Wulder, J. C. White, N. C. Coops, G. W. Hobart, and L. B. Campbell. 2016. "Mass Data Processing of Time Series Landsat Imagery: Pixels to Data Products for Forest Monitoring." *International Journal of Digital Earth* 9 (11): 1035–1054. doi: 10.1080/17538947.2016.1187673.

Hosoi, F., Y. Nakai, and K. Omasa. 2009. "Estimating the Leaf Inclination Angle Distribution of the Wheat Canopy Using a Portable Scanning Lidar." *Journal of Agricultural Meteorology* 65 (3): 297–302.

Husch, B., C. I. Miller, and T. W. Beers. 1982. *Forest Mensuration*. 3rd ed. New York: John Wiley & Sons. ISBN 0471044237.

Jayathunga, S., T. Owari, and S. Tsuyuki. 2018. "Evaluating the Performance of Photogrammetric Products Using Fixed-Wing UAV Imagery Over a Mixed Conifer-Broadleaf Forest: Comparison with Airborne Laser Scanning." *Remote Sensing* 10: 187. doi:10.3390/rs10020187.

Jensen, J., and A. Mathews. 2016. "Assessment of Image-Based Point Cloud Products to Generate a Bare Earth Surface and Estimate Canopy Height in a Woodland Ecosystem." *Remote Sensing* 8: 50–63. doi: 10.3390/rs8010050.

Ke, Y., L. Quachenbush, and J. Im. 2010. "Synergistic Use of Quickbird Multispectral Imagery and LIDAR Data for Object-Based Forest Species Classification." *Remote Sensing of Environment* 114: 1141–1154. doi: 10.1016/j.rse.2010.01.002.

Kelbe, D., J. van Aardt, P. Romanczyk, M. van Leeuwen, and K. Cawse-Nicholson. 2017. "Multiview Marker-Free Registration of Forest Terrestrial Laser Scanner Data with Embedded Confidence Metrics." *IEEE Transactions on Geoscience and Remote Sensing* 55 (2): 729–741. doi: 10.1109/TGRS.2016.2614251.

Keränen, J., M. Maltamo, and P. Packalen. 2016. "Effect of Flying Altitude, Scanning Angle and Scanning Mode on the Accuracy of ALS Based Forest Inventory." *International Journal of Applied Earth Observations and Geoinformation* 52: 349–360. doi: 10.1016/j.jag.2016.07.005.

Khosravipour, A., A. Skidmore, and M. Isenburg. 2016. "Generating Spike-Free Digital Surface Models Using LiDAR Raw Point Clouds: A New Approach for Forestry Applications." *International Journal of Earth Observation and Geoinformation* 52: 104–114. doi: 10.1016/j.jag.2016.06.005.

Kim, T., and I. Dowman. 2006. "Comparison of Two Physical Sensor Models for Satellite Images: Position-Rotation Model and Orbit-Attitude Model." *The Photogrammetric Record* 21 (114): 110–123.

Korhonen, L., K. T. Korhonen, M. Rautiainen, and P. Stenberg. 2006. "Estimation of Forest Canopy Cover: A Comparison of Field Measurement Techniques." *Silva Fennica* 40 (4): 577–588. http://www.metla.fi/silvafennica/full/sf40/sf404577.pdf.

Kratky, V. 1989. "On-line Aspects of Stereophotogrammetric Processing of SPOT Images." *Photogrammetric Engineering & Remote Sensing* 55 (3): 311–316.

Kukkonen, M., M. Maltamo, and P. Packalen. 2017. "Image Matching as a Data Source for Forest Inventory – Comparison of Semi-Global Matching and Next-Generation Automatic Terrain Extraction Algorithms in a Typical Managed Boreal Forest Environment." *International Journal of Applied Earth Observation and Geoinformation* 60: 11–21.

Lague, D., N. Brodu, and J. Leroux. 2013. "Accurate 3D Comparison of Complex Topography with Terrestrial Laser Scanner: Application to the Rangitikei Canyon (N-Z)." *ISPRS Journal of Photogrammetry and Remote Sensing* 82: 10–26. doi: 10.1016/j.isprsjprs.2013.04.009.

Lee, C.-C., and C.-K. Wang. 2018. "Effect of Flying Altitude and Pulse Repetition Frequency on Laser Scanner Penetration Rate for Digital Elevation Model Generation in a Tropical Forest." *GIScience and Remote Sensing* 55 (6): 817–838.

Li, C., S. Zhao, Q. Wang, and W. Shi. 2018. "Uncertainty Modelling and Analysis of Surface Area Calculation Based on a Regular Grid Digital Elevation Model (DEM)." *International Journal of Geographical Information Science* 32 (9): 1837–1859.

Lisein, J., M. Pierrot-Deseilligny, S. Bonnet, and P. Lejeune. 2013. "A Photogrammetric Workflow for the Creation of a Forest Canopy Height Model from Small Unmanned Aerial System Imagery." *Forests* 4: 922–944. doi:10.3390/f4040922.

Liu, J., X. Liang, J. Hyyppä, X. Yu, M. Lehtomäki, J. Pyörälä, L. Zhu, Y. Wang, and R. Chen. 2017. "Automated Matching of Multiple Terrestrial Laser Scans for Stem Mapping Without the Use of Artificial References." *International Journal of Applied Earth Observation and Geoinformation* 56: 13–23. doi: 10.1016/j.jag.2016.11.003.

Liu, J., A. K. Skidmore, S. Jones, T. Wang, M. Heurich, X. Zhu, and Y. Shi. 2018. "Large Off-Nadir Scan Angle of Airborne LiDAR Can Severely Affect the Estimates of Forest Structure Metrics." *ISPRS Journal of Photogrammetry and Remote Sensing* 136: 13–25.

Magnussen, S., T. Nord-Larsen, and T. Riis-Nielsen. 2018. "Lidar Supported Estimators of Wood Volume and Aboveground Biomass from the Danish National Forest Inventory (2012-2016)." *Remote Sensing of Environment* 211: 146–153.

Manferdini, A. M., and F. Remondino. 2010. "Reality-based 3D Modeling, Segmentation and Web-based Visualization". Proc. of EUROMED 2010 Conference, LNCS 6436, Springer-Verlag, pp. 110-124.

Martone, M., P. Rizzoli, C. Wecklich, C. Gonzalez, J.-L. Bueso-Bello, P. Valdo, D. Schulze, M. Zink, G. Krieger, and A. Moreira. 2018. "The Global Forest/Non-Forest Map from TanDEM-X Interferometric SAR Data." *Remote Sensing of Environment* 205: 352–373.

Marx, A., and G. O. Tetteh. 2017. "A Forest Vitality and Change Monitoring Tool Based on RapidEye Imagery." *IEEE Geoscience and Remote Sensing Letters* 14 (6): 801–805.

Matikainen, L., J. Hyyppa, and H. Kaartinen. 2009. "Comparison Between First Pulse and Last Pulse Laser Scanner Data in the Automatic Detection of Buildings." *Photogrammetric Engineering and Remote Sensing* 75 (2): 133–146.
McKeown, D. M., T. Bulwinkle, S. Cochran, W. Harvey, C. McGlone, and J. A. Shufelt. 2000. "Performance Evaluation for Automatic Feature Extraction." *International Archives of Photogrammetry and Remote Sensing* 33 (B2): 379–394.
Meddens, A. J. H., L. A. Vierling, J. U. H. Eitel, J. S. Jennewein, J. C. White, and M. A. Wulder. 2018. "Developing 5 m Resolution Canopy Height and Digital Terrain Models From WorldView and ArcticDEM Data." *Remote Sensing of Environment* 218: 174–188.
Mitchell, H. L., and R. G. Chadwick. 1999. "Digital Photogrammetric Concepts Applied to Surface Deformation Studies." *Geomatica* 53 (4): 405–414.
Moratto, Z. M., M. J. Broxton, R. A. Beyer, M. Lundy, and K. Husmann. 2010. "Ames Stereo Pipeline, NASA's Open Source Automated Stereogrammetry Software". In: 41st Lunar and Planetary Science Conference Abstracts, p. 2364.
Morino, C., S. J. Conway, M. R. Balme, J. Hillier, C. Jordan, P. Saemundsson, and T. Argles. 2018. "Debris-flow Release Processes Investigated Through the Analysis of Multi-Temporal LiDAR Datasets in North-Western Iceland." *Earth Surface Processes and Landforms*. doi: 10.1002/esp.4488.
Mostafa, Y. 2017. "A Review on Various Shadow Detection and Compensation Techniques in Remote Sensing Images." *Canadian Journal of Remote Sensing* 43 (6): 545–562. doi: 10.1080/07038992.2017.1384310.
Navarro, J. A., A. Fernandez-Landa, J. L. Tome, M. L. Guillen-Climent, and J. C. Ojeda. 2018. "Testing the Quality of Forest Variable Estimation Using Dense Image Matching: a Comparison with Airborne Laser Scanning in a Mediterranean Pine Forest." *International Journal of Remote Sensing* 39 (14): 4744–4760.
Noujdina, N. V., and S. L. Ustin. 2008. "Mapping Downy Brome (*Bromus tectorum*) Using Multidate AVIRIS Data." *Weed Science* 56: 173–179. doi: 10.1614/WS-07-009.1.
Päivinen, R., M. Nousiainen, and K. T. Korhonen. 1992. "Puutunnusten Mittaamisen Luotettavuus." *English Summary: Accuracy of Certain Tree Measurements. Folia Forestalia* 787: 18 pages. ISBN: 951-40-1197-X.
Parente, C., and M. Pepe. 2018. ""Uncertainty in Landslides Volume Estimation Using DEMs Generated by Airborne Laser Scanner and Photogrammetry Data". *International Archives of the Photogrammetry. Remote Sensing and Spatial Information Sciences* 42 (3/W4): 397–404. doi: 10.5194/isprs-archives-XLII-3-W4-397-2018.
Pateraki, M. 2005. "Adaptive Multi-Image Matching Algorithm for DSM Generation From Airborne Linear Array CCD Data". Ph.D. thesis, Diss. ETH Zurich, Nr. 15915, Institute of Geodesy and Photogrammetry, Mitteilung No. 86.
Pateraki, M., and E. Baltsavias. 2002. "Adaptive Multi-Image Matching Algorithm for the Airborne Digital Sensor ADS40". In Proc. of Asian Conference on GIS, GPS, Aerial Photography and Remote Sensing (MapAsia 2002), August 7–9, Bangkok, Thailand.
Pearse, G. D., J. P. Dash, H. J. Persson, and M. S. Watt. 2018. "Comparison of High-Density LiDAR and Satellite Photogrammetry for Forest Inventory." *ISPRS Journal of Photogrammetry and Remote Sensing* 142: 257–267.
Persson, H. J., and E. S. Fransson. 2016. "Estimating Site Index from Short-Term TanDEM-X Canopy Height Models." *IEEE Journal of Selected Topics in Applied Earth Observations and Remote Sensing* 9 (8): 3598–3606. doi: 10.1109/JSTARS.2016.2563158.
Pierrot-Deseilligny, M., and N. Paparoditis. 2006. "A Multiresolution and Optimization-Based Image Matching Approach: An Application to Surface Reconstruction from SPOT5-HRS Stereo Imagery". *International Archives of Photogrammetry. Remote Sensing and Spatial Information Sciences* 36 (1/W41): 5 pages.
Poli, D. 2005. "Modelling of Spaceborne Linear Array Sensors". Ph.D. thesis, Institute of Geodesy and Photogrammetry, ETH Zurich, Switzerland. ISBN 3-906467-50-3, Mitteilungen Nr.85, 217 pages.
Poli, D. 2007. "A Rigorous Model for Spaceborne Linear Array Sensors." *Photogrammetric Engineering & Remote Sensing* 73 (2): 187–196.
Poli, D., and T. Toutin. 2012. "Review of Developments in Geometric Modelling for High Resolution Satellite Pushbroom Sensors." *The Photogrammetric Record* 27 (137): 58–73.
Pouliot, D. A., D. J. King, F. W. Bell, and D. G. Pitt. 2002. "Automated Tree Crown Detection and Delineation in High-Resolution Digital Camera Imagery of Coniferous Forest Regeneration." *Remote Sensing of Environment* 82: 322–334.
Puliti, S., S. Saarela, T. Gobakken, G. Stahl, and E. Naesset. 2018. "Combining UAV and Sentinel-2 Auxiliary Data for Forest Growing Stock Volume Estimation Through Hierarchical Model-Based Inference." *Remote Sensing of Environment* 204: 485–497.
Qin, R. 2016. "RPC Stereo Processor (RSP) – A Software Package for Digital Surface Model and Orthophoto Generation from Satellite Stereo Imagery". *ISPRS Annals of the Photogrammetry. Remote Sensing and Spatial Information Sciences III* 1: 77–82. doi: 10.5194/isprsannals-III-1-77-2016.
Qin, R., J. Tian, and P. Reinartz. 2016. "3D Change Detection – Approaches and Applications." *ISPRS Journal of Photogrammetry and Remote Sensing* 122: 41–56.
Rahlf, J., J. Breidenbach, S. Solberg, E. Naesset, and R. Astrup. 2014. "Comparison of Four Types of 3D Data for Timber Volume Estimation." *Remote Sensing of Environment* 155: 325–333.

Reiche, J., E. Hamunyela, J. Verbesselt, D. Hoekman, and M. Herold. 2018. "Improving Near-Real Time Deforestation Monitoring in Tropical Dry Forests by Combining Dense Sentinel-1 Time Series with Landsat and ALOS-2 PALSAR-2." *Remote Sensing of Environment* 204: 147–161.

Remondino, F., S. Del Pizzo, T. Kersten, and S. Troisi. 2012. "Low-Cost and Open-Source Solutions for Automated Image Orientation – A Critical Overview". Proc. EuroMed 2012 Conference, LNCS 7616, Springer, Heidelberg, pp. 40–54.

Remondino, F., M. G. Spera, E. Nocerino, F. Menna, and F. Nex. 2014. "State of the Art in High Density Image Matching." *The Photogrammetric Record* 29 (146): 144–166. doi: 10.1111/phor.12063.

Ressl, C., H. Brockmann, G. Mandlburger, and N. Pfeifer. 2016. "Dense Image Matching vs. Airborne Laser Scanning – Comparison of Two Methods for Deriving Terrain Models". *Photogrammetrie, Fernerkundung, Geoinformation* 2: 57–73. doi: 10.1127/pfg/2016/0288.

Rosenholm, D., and K. Torlegard. 1988. "Three-Dimensional Absolute Orientation of Stereo Models Using Digital Elevation Models." *Photogrammetric Engineering & Remote Sensing* 54 (10): 1385–1389.

Rothermel, M., K. Wenzel, D. Fritsch, and N. Haala. 2012. "SURE: Photogrammetric Surface Reconstruction from Imagery." In Proceedings of LowCost3D Workshop, Berlin.

Rupnik, E., M. Daakir, and M. Pierrot-Deseilligny. 2017. "MicMac – A Free, Open-Source Solution for Photogrammetry". *Open Geospatial Data, Software and Standards* 2 (14): 1–9. doi: 10.1186/s40965-017-0027-2.

Rupnik, E., M. Pierrot-Deseilligny, and A. Delorme. 2018. "3D Reconstruction from Multi-View VHR-Satellite Images in MicMac." *ISPRS Journal of Photogrammetry and Remote Sensing* 139: 201–211.

Rutzinger, M., F. Rottensteiner, and N. Pfeifer. 2009. "A Comparison of Evaluation Techniques for Building Extraction from Airborne Laser Scanning." *IEEE Journal of Selected Topics in Applied Earth Observations and Remote Sensing* 2 (1): 11–20. doi: 10.1109/JSTARS.2009.2012488.

Sadeghi, Y., B. St-Onge, B. Leblon, J.-F. Prieur, and M. Simard. 2018. "Mapping Boreal Forest Biomass from a SRTM and TanDEM-X Based on Canopy Height Model and Landsat Spectral Indices." *International Journal of Applied Earth Observation and Geoinformation* 68: 202–213.

Sambatti, J., D. Crouse, B. MacArthur, and I. Moss. 2017. "An Operational High-Resolution Forest Inventory". GIM International. https://www.gim-international.com/content/article/an-operational-high-resolution-forest-inventory [Last access on: 14/11/2018].

Sankey, T., J. Donager, J. McVay, and J. B. Sankey. 2017. "UAV Lidar and Hyperspectral Fusion for Forest Monitoring in the Southwestern USA." *Remote Sensing of Environment* 195: 30–43.

Scaioni, M., L. Barazzetti, M. Corti, J. Crippa, R. S. Azzoni, D. Fugazza, M. Cernuschi, and G. A. Diolaiuti. 2018. ""Integration of Terrestrial and UAV Photogrammetry for the Assessment of Collapse Risk in Alpine Glaciers". *The International Archives of the Photogrammetry, Remote Sensing and Spatial Information Sciences XLII* 3 (W4): 445–452. doi: 10.5194/isprs-archives-XLII-3-W4-445-2018.

Schlund, M., F. von Poncet, S. Kuntz, H.-D. V. Boehm, D. H. Hoekman, and C. Schmullius. 2016. "TanDEM-X Elevation Model Data for Canopy Height and Aboveground Biomass Retrieval in a Tropic Peat Swamp Forest." *International Journal of Remote Sensing* 37 (21): 5021–5044. doi: 10.1080/01431161.2016.1226001.

Schönberger, J. L., and J.-M. Frahm. 2016. "Structure-from-Motion Revisited". In Proceedings of IEEE Conference on Computer Vision and Pattern Recognition (CVPR), pp. 4104-4113. doi: 10.1109/CVPR.2016.445.

Schönberger, J. L., E. Zheng, M. Pollefeys, and J.-M. Frahm. 2016. "Pixelwise View Selection for Unstructured Multi-View Stereo". In Proceedings of European Conference on Computer Vision (ECCV).

Sedaghat, A., and A. A. Naeini. 2018. "DEM Orientation Based on Local Feature Correspondence with Global DEMs." *GIScience and Remote Sensing* 55 (1): 110–129.

Senf, C., D. Pflugmacher, P. Hostert, and R. Seidl. 2017. "Using Landsat Time Series for Characterizing Forest Disturbance Dynamics in the Coupled Human and Natural Systems of Central Europe." *ISPRS Journal of Photogrammetry and Remote Sensing* 130: 453–463.

Shean, D. E., O. Alexandrov, Z. M. Moratto, B. E. Smith, I. R. Joughin, C. Porter, and P. Morin. 2016. "An Automated, Open-Source Pipeline for Mass Production of Digital Elevation Models (DEMs) from Very-High-Resolution Commercial Stereo Satellite Imagery." *ISPRS Journal of Photogrammetry and Remote Sensing* 116: 101–117. doi: 10.1016/j.isprsjprs.2016.03.012.

Shufelt, J. A. 1999. "Performance Evaluation and Analysis of Monocular Building Extraction from Aerial Imagery." *IEEE Transactions on Pattern Analysis and Machine Intelligence* 21 (4): 311–326.

Simpson, J. E., T. E. L. Smith, and M. J. Wooster. 2017. "Assessment of Errors Caused by Forest Vegetation Structure in Airborne LiDAR-Derived DTMs." *Remote Sensing* 9: 1101. doi: 10.3390/rs9111101.

Stepper, C., C. Straub, and H. Pretzsch. 2015. "Assessing Height Changes in a Highly Structured Forest Using Regularly Acquired Aerial Image Data." *Forestry* 88 (3): 304–316.

Tao, C. V., and Y. Hu. 2001. "A Comprehensive Study of the Rational Function Model for Photogrammetric Processing." *Photogrammetric Engineering & Remote Sensing* 66 (12): 1477–1485.

Tarvydas, A. 1983. "Terrain Approximation by Triangular Facets". In Proceedings of Sixth International Symposium on Automated Cartography. Ottawa, Canada.

Tian, J., T. Schneider, C. Straub, F. Kugler, and P. Reinartz. 2017. "Exploring Digital Surface Models from Nine Different Sensors for Forest Monitoring and Change Detection." *Remote Sensing* 9 (287). doi: 10.3390/rs9030287.
Toutin, T. 2004. "Review Article: Geometric Processing of Remote Sensing Images: Models, Algorithms and Methods." *International Journal of Remote Sensing* 25 (10): 1893–1924.
Tran, T. H. G., C. Ressl, and N. Pfeifer. 2018. "Integrated Change Detection and Classification in Urban Areas Based on Airborne Laser Scanning Point Clouds." *Sensors* 18: 448. doi: 10.3390/s18020448.
Tsai, V. J. D. 1993. "Delaunay Triangulations in TIN Creation: An Overview and a Linear-Time Algorithm." *International Journal of Geographical Information Systems* 7 (6): 501–524. doi: 10.1080/02693799308901979.
Van Leeuwen, M., and M. Nieuwenhuis. 2010. "Retrieval of Forest Structural Parameters Using LiDAR Remote Sensing." *European Journal of Forest Research* 129 (4): 749–770. doi: 10.1007/s10342-010-0381-4.
Vauhkonen, J., M. Holopainen, V. Kankare, M. Vastaranta, and R. Viitala. 2016. "Geometrically Explicit Description of Forest Canopy Based on 3D Triangulations of Airborne Laser Scanning Data." *Remote Sensing of Environment* 173: 248–257. doi: 10.1016/j.rse.2015.05.009.
Vo, A.-V., D. F. Laefer, and M. Bertolotto. 2016. "Airborne Laser Scanning Data Storage and Indexing: State-of-the-art Review." *International Journal of Remote Sensing* 37 (24): 6187–6204. doi: 10.1080/01431161.2016.1256511.
Wagner, F. H., M. P. Ferreira, A. Sanchez, M. C. M. Hirye, M. Zortea, E. Gloor, O. L. Phillips, C. R. de Souza Filho, Y. E. Shimabukuro, and L. E. O. C. Aragao. 2018. "Individual Tree Crown Delineation in a Highly Diverse Tropical Forest Using Very High Resolution Satellite Images." *ISPRS Journal of Photogrammetry and Remote Sensing* 145 (Part B): 362–377.
Wallis, R. 1976. "An Approach to the Space Variant Restoration and Enhancement of Images". Proc. of Symposium on Current Mathematical Problems in Image Science, Monterey, CA, USA.
Wang, Y., J. Hyyppä, X. Liang, H. Kaartinen, X. Yu, E. Lindberg, J. Holmgren, et al. 2016. "International Benchmarking of the Individual Tree Detection Methods for Modeling 3-D Canopy Structure for Silviculture and Forest Ecology Using Airborne Laser Scanning." *IEEE Transactions on Geoscience and Remote Sensing* 54 (9): 5011–5027. doi: 10.1109/TGRS.2016.2543225.
Waser, L. T., E. Baltsavias, K. Ecker, H. Eisenbeiss, E. Feldmeyer-Christe, C. Ginzler, M. Küchler, P. Thee, and L. Zhang. 2008a. "High-Resolution Digital Surface Models (DSMs) for Modelling Fractional Shrub/Tree Cover in a Mire Environment." *International Journal of Remote Sensing* 29 (5): 1261–1276.
Waser, L. T., E. Baltsavias, K. Ecker, H. Eisenbeiss, E. Feldmeyer-Christe, C. Ginzler, M. Küchler, and L. Zhang. 2008b. "Assessing Changes of Forest Area and Shrub Encroachment in a Mire Ecosystem Using Digital Surface Models and CIR Aerial Images." *Remote Sensing of Environment* 112: 1956–1968.
Waser, L. T., E. Baltsavias, H. Eisenbeiss, C. Ginzler, A. Gruen, M. Kuechler, and P. Thee. 2007. "Change Detection in Mire Ecosystem: Assessing Changes of Forest Areas Using Airborne Remote Sensing Data." *International Archives of Photogrammetry, Remote Sensing and Spatial Information Sciences* 36 (7-C50): 313–318.
Wastlund, A., J. Holmgren, E. Lindberg, and H. Olsson. 2018. "Forest Variable Estimation Using a High Altitude Single Photon Lidar System." *Remote Sensing* 10: 1422. doi: 10.3390/rs10091442.
Wheaton, J. M., J. Brasington, S. E. Darby, and D. A. Sear. 2010. "Accounting for Uncertainty in DEMs from Repeat Topographic Surveys: Improved Sediment Budgets." *Earth Surface Processes and Landforms* 35: 136–156. doi: 10.1002/esp.1886.
White, J. C., P. Tompalski, N. C. Coops, and M. A. Wulder. 2018. "Comparison of Airborne Laser Scanning and Digital Stereo Imagery for Characterizing Forest Canopy Gaps in Coastal Temperate Rainforests." *Remote Sensing of Environment* 208: 1–14.
Wu, B., B. Yu, Q. Wu, Y. Huang, Z. Chen, and J. Wu. 2016. "Individual Tree Crown Delineation Using Localized Contour Tree Method and Airborne LiDAR Data in Coniferous Forests." *International Journal of Applied Earth Observation and Geoinformation* 52: 82–94. doi: 10.1016/j.jag.2016.06.003.
Xiao, W., S. Xu, S. Oude Elberink, and G. Vosselman. 2016. "Individual Tree Crown Modeling and Change Detection from Airborne Lidar Data." *IEEE Journal of Selected Topics in Applied Earth Observations and Remote Sensing* 9 (8): 3467–3477. doi: 10.1109/JSTARS.2016.2541780.
Zhang, L. 2005. "Automatic Digital Surface Model (DSM) Generation from Linear Array Images". Ph.D. thesis, Institute of Geodesy and Photogrammetry, ETH Zurich, Switzerland. ISBN 3-906467-55-4, Mitteilungen Nr.88, 219 pages.
Zhang, L., and A. Gruen. 2004. "Automatic DSM Generation from Linear Array Imagery Data." *International Archives of Photogrammetry and Remote Sensing* 35 (B3): 128–133.
Zhang, L., and A. Gruen. 2006. "Multi-Image Matching for DSM Generation from IKONOS Imagery." *ISPRS Journal of Photogrammetry & Remote Sensing* 60: 195–211. doi: 10.1016/j.isprsjprs.2006.01.001.
Zhang, L., S. Kocaman, D. Akca, W. Kornus, and E. Baltsavias. 2006. "Test and Performance Evaluation of DMC Images and New Methods for Their Processing". ISPRS Commission I Symposium, Paris, July 3-6, (only on CD-ROM).
Zheng, G., and M. Moskal. 2012. "Leaf Orientation Retrieval from Terrestrial Laser Scanning (TLS) Data." *IEEE Transactions on Geoscience and Remote Sensing* 50 (10): 3970–3979.
Zhu, Z. 2017. "Change Detection Using Landsat Time Series: A Review of Frequencies, Preprocessing, Algorithms, and Applications." *ISPRS Journal of Photogrammetry and Remote Sensing* 130: 370–384.